BOND CHARECTERISTICS OF FRP COMPOSITE WITH CONCRETE SUBSTRATE

A Dissertation submitted
In partial Fulfilment of the Requirements for
the award of degree of

MASTERS OF ENGINEERING

IN

CIVIL (STRUCTURES)

ENGINEERING

Submitted by

PANKAJ BHARDWAJ
(ROLL NO. 801222010)

Under the guidance of

Dr. PREM PAL BANSAL
Assistant Professor

CIVIL ENGINEERING DEPARTMENT

THAPAR UNIVERSITY, PATIALA- 147004

JULY 2014

CERTIFICATE

Certified that the thesis **"BOND CHARACTERISTICS OF FRP COMPOSITE WITH CONCRETE SUBSTRATE"** which is submitted by **Mr. Pankaj Bhardwaj**, in fulfilment of the requirement for the award of the degree of Master of Technology in the **Department of Civil Engineering (CED),** Thapar University, Patiala, is a record of the candidate's own independent and original research work carried out by him under supervision and guidance of **Dr. Prem Pal Bansal**. The matter embodied in this thesis has not been submitted in part or full to any other University or Institute for the award of any degree.

Pankaj Bhardwaj

Date: 15/07/2014 **Pankaj Bhardwaj**

It is certified that the above statement made by the student is correct to best of my/our knowledge and belief

(Dr. Prem Pal Bansal)
Guide, Assistant Professor
CED, Thapar University
Patiala-147004

Countersigned by:

(Dr. Naveen Kwatra)
Head, CED
ThaparUniversity
Patiala-147004

(Dr.S.K. Mohapatra)
Dean, Academics Affairs
Thapar University
Patiala 147004

ACKNOWLEDGEMENT

"*One can pay back the loan of gold, but one dies forever in debt to those who are kind***."**

A dissertation cannot be completed without the help of many people who ushered me in going through this difficult path. It would be unfair, if I don't say a word of thanks to all those whose sincere advice made this period a real educative, enlightening, pleasurable and memorable one.

First of all, a special debt of gratitude is owned to my guide **Dr. Prem Pal Bansal** for his gracious efforts and keen pursuits, which has remained as a valuable asset for the successful completion of research work.

I also like to offer my sincere thanks to all faculty members, teaching and non-teaching staff of Civil Engineering Department (CED), and staff of central library, TU, Patiala for their assistance. I am extremely thankful to my friends, Mr. Sukhdeep Singh Mr. Parvinder Singh and Mr. Gurpreet Singh and all other manpower for helping me to carry out experimental work.

Pankaj Bhardwaj
M.E Civil (Structures)
Regd. No. 801222010

ABSTRACT

Many existing structures nowadays are unable to give their services effectively. Due to various reasons, they get deteriorated or get damaged much before the time for which they are designed for. The evaluation of the damage can be measured by various destructive and non destructive tests. Such damaged structures need to be retrofitted. Various structures like bridges, dams, for which rehabilitation is very difficult, in such cases retrofitting can be used as an effective measure. There are various methods for retrofitting like jacketing, shear wall, infill wall etc apart from the conventional methods. Out of all these methods jacketing using fibre composites are getting popularity these days. These FRP composites mostly fail in debonding. Since delamination is a very brittle and sudden failure mechanism without prior to yielding, it must be avoided in practical applications. This nature of the Stress level in interfacial bond between the FRP sheet and the concrete substrate is therefore important to study.

In the present study the research was carried to study the effect of CFRP bond with the concrete substrate. In this study the sheet was pulled from the concrete surface and the slip was measured. The idea behind this test was to find the stress level which leads to its debonding and relate the stresses with those generated at flexural testing. The parameters studied were the different surface preparation. The samples were tested on controlled/undamaged beam and damaged beam. Apart from this grooved and holed samples were also tested. The results of the samples were finally compared to the existing models and previous research.

From the results it was found that by cutting longitudinal grooves and filling them with an appropriate epoxy was an effective substitute for surface preparation, and can cause a great increase in ultimate load of beams compared to those without any surface preparation. The shear failure of concrete was noticed in case of damaged beams. The holed sample did not show appreciable results. The results of the controlled/undamaged beam were compared with the previous researches and were found to be in satisfactory ranges.

CONTENTS

LIST OF FIGURES

LIST OF TABLES

CHAPTER-1 INRTODUCTION

1.1 GENERAL

Today the major challenge which the civil industry is facing is the deterioration of the concrete structures. Reinforced concrete is a very versatile construction material. Properly designed concrete structures are both strong and durable. However, concrete structures are vulnerable to a number of factors that can cause deterioration. Deterioration can result in loss of strength and unsafe conditions. Due to such reasons the service life of the structure has abated considerably leading heavy economical losses. Therefore it is important to have an understanding of the vulnerabilities of concrete structures in order to help minimize long-term repair and maintenance costs. These structures are in dire need of rehabilitation by retrofitting or replacement because of their improper functionality. Retrofitting is the modification of existing structures to make them capable to carry same or more loads for which they are designed for. Practically there are different retrofitting techniques available like external post-tensioning, Base isolators, Supplementary dampers, Tuned mass dampers, Slosh tank, Active control system etc.

An attractive solution is strengthening of the existing structures using FRP composites. High tensile strength, lightweight and corrosion resistance characteristics of FRP make it ideal for retrofitting applications. Many studies have shown that significant increase in stiffness of structural member after they are properly wraped with fibre sheet. The fibres with polymer resin have shown improved strengths and have proved to be the efficient method in retrofitting of some existing structures. However, existing experimental research shows that the theoretical high ultimate capacity of FRP strengthened reinforced concrete (RC) beams often cannot be achieved because of FRP plate debonding or horizontal cracking and subsequent loss of concrete cover below the reinforcing steel. This significantly reduces the strength enhancement provided by the FRP and can create brittle failures. As a result, there is significant concern in the engineering community regarding the safety and effectiveness of externally bonded FRP strengthening of RC structures. Therefore there is dire need of study of debonding mechanism so that the debonding can be clearly understood and measures could be taken to make effective use of FRP

composites. This research is intended towards the debonding criteria of fibre with concrete substrate

1.2 FIBRE-REINFORCED POLYMERS

Fibre-reinforced polymer (FRP), also Fibre-reinforced plastic, is a polymer material which is strengthened with fibres. The fibres are usually glass, carbon, or aramid, although other fibres such as paper or wood or asbestos have been sometimes used. The polymer is usually an epoxy, vinylester or polyester thermosetting plastic, and phenol formaldehyde resins which are still in use. FRPs are commonly used in the aerospace, automotive, marine, and construction industries. Composite materials are engineered or naturally occurring materials made from two or more constituent materials with significantly different physical or chemical properties which remain separate and distinct within the finished structure. Most composites have strong, stiff fibres in a matrix which is weaker and less stiff. The objective is usually to make a component which is strong and stiff, often with a low density. Commercial material commonly has glass or carbon fibres in matrices based on thermosetting polymers, such as epoxy or polyester resins. Sometimes, thermoplastic polymers may be preferred, since they are moldable after initial production. Furthermore, in these composites the reasons for adding the fibres are often complex.

1.3 ADVANTAGES OF FRP'S

Fibre reinforced polymer (FRP) are composites used in almost every type of advanced engineering structure, with their usage ranging from aircraft, helicopters and spacecraft through to boats, ships and offshore platforms and to automobiles, sports goods, chemical processing equipment and civil infrastructure such as bridges and buildings. The usage of FRP composites continues to grow at an impressive rate as these materials are used more in their existing markets and become established in relatively new markets such as biomedical devices and civil structures. The fibre reinforced polymer composites (FRPs) are increasingly being considered as an enhancement and substitute for infrastructure components or systems that are constructed of traditional civil engineering materials, namely concrete and steel. FRP composites are

- Lightweight

- Noncorrosive
- Exhibit high specific strength and specific stiffness
- Are easily constructed
- Can be tailored to satisfy performance requirements.

Due to these advantageous characteristics, FRP composites have been included in rehabilitation of structures through its use as reinforcement in concrete, bridge decks, modular structures, formwork, and external reinforcement for strengthening and seismic upgrade.

The applicability of Fiber Reinforced Polymer (FRP) reinforcements to concrete structures as a substitute for steel bars or prestressing tendons has been studied in numerous research laboratories and professional organizations around the world. FRP reinforcements offer a number of advantages such as corrosion resistance, non-magnetic properties, high tensile strength, lightweight and ease of handling.

1.4 LIMITATIONS

- They generally have a linear elastic response in tension up to failure (described as a brittle failure) and a relatively poor transverse or shear resistance.
- They also have poor resistance to fire and when exposed to high temperatures.
- They lose significant strength upon bending, and they are sensitive to stress-rupture effects.
- Moreover, their cost, whether considered per unit weight or on the basis of force carrying capacity, is high in comparison to conventional steel reinforcing bars or prestressing tendons.
- From a structural engineering viewpoint, the most serious problems with FRP reinforcements are the lack of plastic behaviour and the very low shear strength in the transverse direction. Such characteristics may lead to premature tendon rupture, particularly when combined effects are present.

1.5 SUSTAINABILITY OF FRP's

Solutions and limitations of use have been offered and continuous improvements are expected in the future. The unit cost of FRP reinforcements is expected to decrease

significantly with increased market share and demand. However, even today, there are applications where FRP reinforcements are cost effective and justifiable. Such cases include the use of bonded FRP sheets or plates in repair and strengthening of concrete structures, and the use of FRP meshes or textiles or fabrics in thin cement products. The cost of repair and rehabilitation of a structure is always higher than the cost of the initial structure. Repair generally requires a relatively small volume of repair materials but a relatively high commitment in labor. Moreover the cost of labor in developed countries is so high that the cost of material becomes secondary. Thus the highest the performance and durability of the repair material is, the more cost-effective is the repair. This implies that material cost is not really an issue in repair and that the fact that FRP repair materials are costly is not a constraining drawback. When considering only energy and material resources it appears, on the surface, the argument for FRP composites in a sustainable built environment is questionable. However, such a conclusion needs to be evaluated, advantages present in use of FRP composites related to considerations such as:

- Higher strength
- Lighter weight
- Higher performance
- Longer lasting
- Rehabilitating existing structures and extending their life
- Seismic upgrades
- Defense systems
- Space systems
- Ocean environments

In the case of FRP composites, environmental concerns appear to be a barrier to its feasibility as a sustainable material especially when considering fossil fuel depletion, air pollution, smog, and acidification associated with its production. In addition, the ability to recycle FRP composites is limited and, unlike steel and timber, structural components cannot be reused to perform a similar function in another structure. However, evaluating the environmental impact of FRP composites in infrastructure applications, specifically through life cycle analysis, may reveal direct and indirect benefits that are more competitive than conventional materials. Composite materials

have developed greatly since they were first introduced. However, before composite materials can be used as an alternative to conventional materials as part of a sustainable environment a number of needs remain.

• Availability of standardized durability characterization data for FRP composite materials.

• Integration of durability data and methods for service life prediction of structural members
utilizing FRP composites.

• Development of methods and techniques for materials selection based on life cycle assessments of structural components and systems.

Ultimately composites must be structurally and economically feasible. Numerous studies regarding the structural feasibility of composite materials are widely available in literature . However, limited studies are available on the economic and environmental feasibility of these materials. Additionally, the long term affects of using composite materials needs to be determined. The byproducts of the production, the sustainability of the constituent materials, and the potential to recycle composite materials needs to be assessed in order to determine of composite materials can be part of a sustainable environment.

1.6 COMMERCIALLY AVAILABLE EXTERNALLY BONDED FRP SYSTEMS

FRP systems come in a variety of forms, including wet layup systems and precured systems. FRP system forms can be categorized based on how they are delivered to the site and installed. The FRP system and its form should be selected based on the acceptable transfer of structural loads and the ease and simplicity of application.

1.6.1 Wet Layup Systems

Wet layup FRP systems consist of dry unidirectional or multidirectional fiber sheets or fabrics impregnated with a saturating resin on site. The saturating resin along with the compatible primer and putty bonds the FRP sheets to the concrete surface. Wet layup systems are saturated in place and cured in place and, is similar to cast-in-place concrete. Three common types of wet layup systems are listed as follows:

1. Dry unidirectional fiber sheets where the fibers run predominantly in one planar direction;
2. Dry multidirectional fiber sheets or fabrics where the fibers are oriented in at least two planar directions; and
3. Dry fiber tows that are wound or otherwise mechanically applied to the concrete surface. The dry fiber tows are impregnated with resin on site during the winding operation.

1.6.2 Prepreg Systems

Prepreg FRP systems consist of partially cured unidirectional or multidirectional fiber sheets or fabrics that are preimpregnated with a saturating resin in the manufacturer's facility. Prepreg systems are bonded to the concrete surface with or without an additional resin application, depending on specific system requirements. Prepreg systems are saturated off-site and, like wet layup systems, cured in place. Prepreg systems usually require additional heating for curing. Three common types of prepreg FRP systems are:
1. Preimpregnated unidirectional fiber sheets where the fibers run predominantly in one planar direction;
2. Preimpregnated multidirectional fiber sheets or fabrics where the fibers are oriented in at least two planar directions; and
3. Preimpregnated fiber tows that are wound or otherwise mechanically applied to the concrete surface.

1.6.3 Precured Systems

Precured FRP systems consist of a wide variety of composite shapes manufactured off site. Typically, an adhesive, along with the primer and putty, is used to bond the precured shapes to the concrete surface. The system manufacturer should be consulted for recommended installation procedures. Precured systems are analogous to precast concrete. Three common types of precured systems are:
1. Precured unidirectional laminate sheets, typically delivered to the site in the form of large flat stock or as thin ribbon strips coiled on a roll;
2. Precured multidirectional grids, typically delivered to the site coiled on a roll; and
3. Precured shells, typically delivered to the site in the form of shell segments cut longitudinally so they can be opened and fitted around columns or other members;

multiple shell layers are bonded to the concrete and to each other to provide seismic confinement.

1.6.4 Near-Surface-Mounted (NSM) Systems

Surface embedded (NSM) FRP systems consist of circular or rectangular bars or plates installed and bonded into grooves made on the concrete surface. A suitable adhesive is used to bond the FRP bar into the groove, and is cured in-place. Two common FRP bar types used for NSM applications are:

1. Round bars usually manufactured using pultrusion processes, typically delivered to the site in the form of single bars or in a roll depending on bar diameter; and
2. Rectangular bars and plates usually manufactured using pultrusion processes, typically delivered to the site in a roll

1.7 INSTALLATION PROCESS OF FRP'S

Procedures for installing FRP systems have been developed by the system manufacturers and often differ between systems. In addition, installation procedures can vary within a system, depending on the type and condition of the structure. Deviations from the procedures developed by the FRP system manufacturer should not be allowed without consulting with the manufacturer. The behaviour of concrete members strengthened or retrofitted with FRP systems is highly dependent on a sound concrete substrate and proper preparation and profiling of the concrete surface. An improperly prepared surface can result in debonding or delamination of the FRP system before achieving the design load transfer. Substrate preparation can generate noise, dust, and disruption to building occupants.

1.7.1 Substrate Repair

All problems associated with the condition of the original concrete and the concrete substrate that can compromise the integrity of the FRP system should be addressed before surface preparation begins. The FRP system manufacturer should be consulted on the compatibility of the FRP system with materials used for repairing the substrate.

1.7.2 Corrosion-Related Deterioration

Externally bonded FRP systems should not be applied to concrete substrates suspected of containing corroded reinforcing steel. The expansive forces associated

with the corrosion process are difficult to determine, and could compromise the structural integrity of the externally applied FRP system.

1.7.3 Injection of Cracks

Cracks that are 0.010 in. (0.3 mm) and wider can affect the performance of the externally bonded FRP system through delamination or fibre crushing. Consequently, cracks wider than 0.010 in. (0.3 mm) should be pressure injected with epoxy before FRP installation. Smaller cracks exposed to aggressive environments may require resin injection or sealing to prevent corrosion of existing steel reinforcement.

1.7.4 Surface Preparation

Surface preparation requirements should be based on the intended application of the FRP system. Applications can be categorized as bond-critical or contact-critical. Bond-critical applications, such as flexural or shear strengthening of beams, slabs, columns, or walls, require an adhesive bond between the FRP system and the concrete.

1.8 BOND AND DELAMINATION

Over the past few decade we have seen external bonding of fibre reinforced polymer (FRP) plates or sheets has emerged as a popular method for the strengthening of reinforced concrete (RC) structures.

Debonding failure of FRP reinforced RC beams usually takes place via areas of high stress concentrations. These are usually associated with FRP material termination and the presence/appearance of cracks in the concrete substrate (Fig. 1.1). The path of debonding propagation (Fig. 1.2) depends on properties of the substrate concrete, FRP, and interface (adhesive) and follows the path of least resistance. FRP debonding through the concrete substrate was identified as an important failure mode because it occurs at lighter load levels and the failure is very brittle. Early research indicated improper selection of adhesives increases the likelihood of failure, and that the failure behaviour was heavily dependent on the existing steel reinforcing ratio and the type of FRP reinforcement

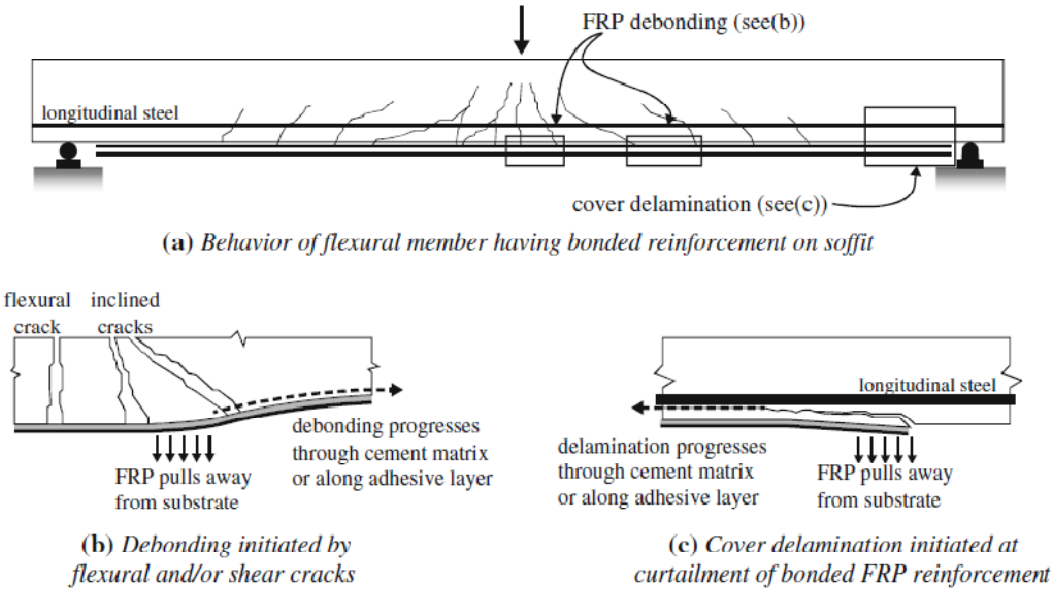

Fig 1.1 Debonding And Delamination of Externally Bonded FRP Systems (ACI 440R.2-08)

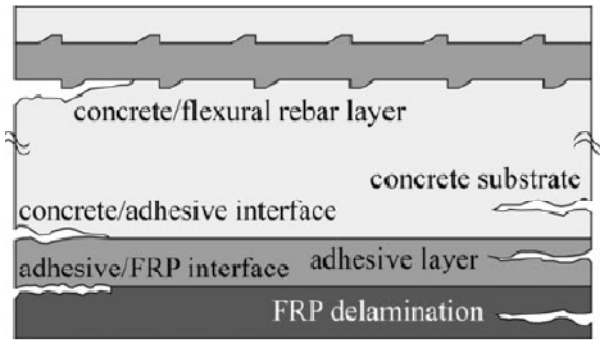

Fig. 1.2 Paths of Debonding Propagation.

It has also been shown that extending the FRP reinforcement as much as possible toward the supports decreases the potential of debonding, but does not eliminate it. Interfacial debonding may occur as shown schematically in Figure 1.2 through

• Concrete cover separation,

• Plate-end interfacial debonding,

• Intermediate (flexure or flexure shear) crack induce interfacial debonding,

• Critical diagonal crack induced interfacial debonding.

Loss of composite action resulting from unevenness of the concrete surface is quite easy to conceptualize. However, failure resulting from debonding in the anchorage zone or in the vicinity of cracks is not as intuitive and the mechanisms are more difficult to understand.

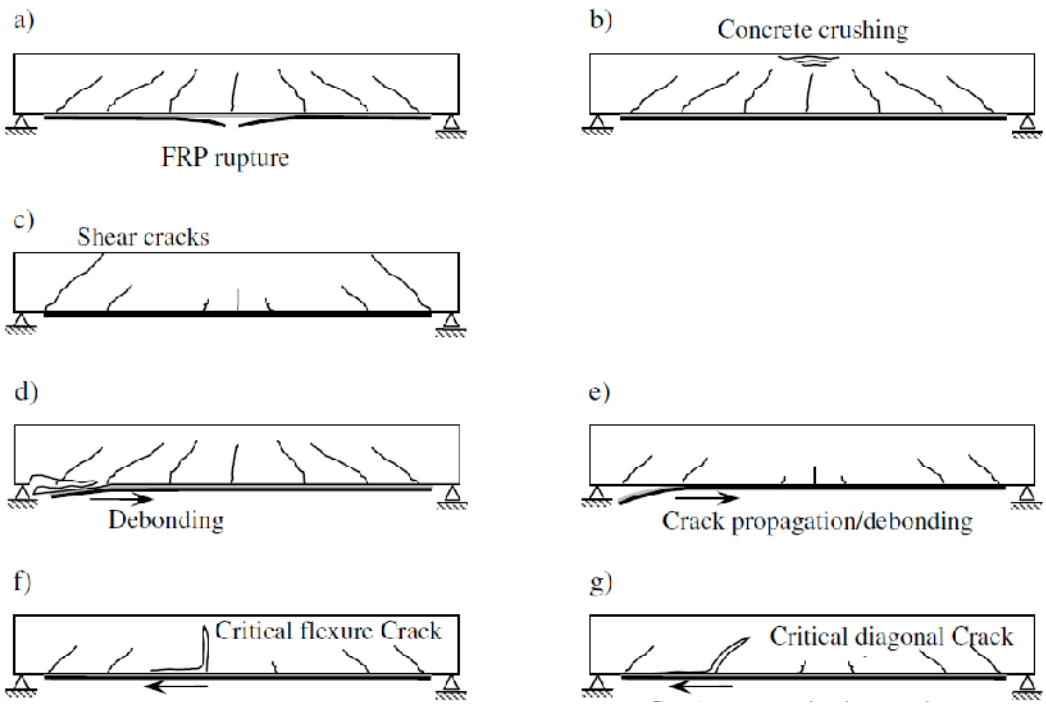

Fig. 1.3 Failure Modes of RC Beams with Bonded FRP-Strips (Teng et al. 2002; Lu et al. 2005; Oehler et al. 2003; Teng et al. 2004)

In fig1.3 the various figures represent:

a) Flexure failure by FRP ruptures. b) Flexure failure by concrete crushing. c) Shear failure d) Concrete cover separation. e) Plate-end interfacial debonding; f) Flexure crack-induced interfacial debonding. g) Critical diagonal crack-induced interfacial debonding

Failure initiating in the uncracked anchorage zone may be referred to as ripping or end peel failure is characterized by the formation of an inclined crack from the soffit of the beam to the level of the conventional flexural reinforcement. Cracking proceeds along the level of the internal reinforcement until the laminate is completely separated from the beam. This failure mode is found to occur frequently in beams where the laminate is terminated far from the supports and is commonly encountered for beams strengthened with steel plates. Peeling of the composite laminate initiating at the location of a shear/flexure crack (defined above as intermediate crack-induced interfacial debonding) is characterized by a relative vertical displacement of the FRP across the crack opening. Once this has occurred there is a vertical component of the force in the FRP that puts the concrete in direct tension. When this vertical component exceeds the tensile strength of the concrete, cracking propagates back toward the

support. The strength of the adhesive is not a limiting factor in this mode since it is stronger than the concrete. The concrete that remains bonded to the laminate after failure demonstrates crack progression through the concrete.

The actual distribution of bond stress in an FRP laminate is complicated by cracking of the substrate concrete. In reinforced concrete members having relatively long shear spans or where the end peeling has been effectively mitigated, debonding may initiate at flexural cracks, flexural/shear cracks, or both, near the region of maximum moment. Under loading, these cracks open and induce high interfacial shear stress that causes FRP debonding that propagates across the shear span in the direction of decreasing moment. In the case of direct pull off test the modes of failure depends merely on the interfaces which exist in the bonding system.

The different modes of failure can be

1. Interfacial zone between concrete and epoxy fail
    - Failure of epoxy. Visible hairline cracks propagate in failure zone, which can be further accompanied by delamination of FRP while the concrete surface remains intact
    - Failure of concrete. The bond between FRP and epoxy is though intact but during delaminating concrete fails in shear.
2. Interfacial zone between epoxy and FRP This occurs with cracks on epoxy and FRP rupture.

The pull test not only delivers the ultimate load of the FRP to- concrete interface, but also has been used to determine the local bond–slip behaviour of the interface .

1.9 OBJECTIVES OF RESEARCH

This objective of this research is to understand the FRP-concrete bond behaviour. Different parameters which were studied differ in surface preparation, includes

- Samples on undamaged/controlled beam
- Samples with grooves on beam
- Samples with holes on beam
- Samples on damaged beam

The effort is made to understand the effects of these parameter in ultimate load carrying capacity of bond. The strain distribution along FRP and bond slip analysis is the key points to be studied.

1.10 ORIENTATION OF THESIS

The thesis report consists of five chapters:

Chapter 1- Provides introduction on FRP's composites. Their advantages, limitation and sustainability of use are discussed in detail. Furthermore bond delamination modes are also discussed.

Chapter 2- Deals with the study of various researchers on FRP debonding in direct pull test.

Chapter 3- Details the scheme of experimentation, materials used and variables involved. Information about adhesives, fibres is also discussed in this chapter.

Chapter 4- Presents the results, and their analysis for strain distribution and bond slip relations are done.

Chapter 5- Summarizes and concludes the findings of the study. Few recommendations for further studies are also discussed.

References are placed at the end.

CHAPTER 2 LITERATURE REVIEW

2.1 INTRODUCTION

Studying the debonding characteristics has become a subject of vital importance in many countries. It is very important to understand the stress distribution along FRP's and critical stresses which leads to debonding. Since delamination is a very brittle failure mechanism, it must be avoided in practical applications. Bonding depends on mechanical and physical properties of concrete, composite and adhesive. This chapter includes the study of various researches where bond slips relationships were analysed along with the strain distribution on FRP sheets.

2.2 RESEARCH FINDINGS

Mazzotti et al. (2004) conducted an experimental study on FRP and concrete delamination. In this paper, four specimens with different bonding lengths have been prepared. A number of closely spaced strain gages have been used to measure strains along the FRP plate. Moreover, LVDT transducers have been used to measure displacements. Starting from experimental data, average shear stresses between two subsequent strain guages and corresponding shear slips were computed.

The (estimated) value of maximum transmissible load by an anchorage of infinite length is used to define the value of fracture energy of interface law. Fracture energy of constitutive interface law which is an important condition to be satisfied to predict the correct value of maximum transmissible load through the interface. Moreover, the softening branch, where experimental results are very scattered, is strongly influenced by the value of fracture energy.

Four different bonded lengths have been tested: 50, 100, 200 and 400 mm. The detail of the specimen and experimental setup have been explained in the fig 2.1. For composite plates, CFRP Sika CarboDur S plates 50 mm wide and 1.2 mm thick have been used. According to technical data provided by the producer, plates have a carbon fiber volumetric content equal to 70 per cent, an epoxy matrix, a minimum tensile strength of 2200 MPa and a mean elastic modulus Ep = 165000 MPa

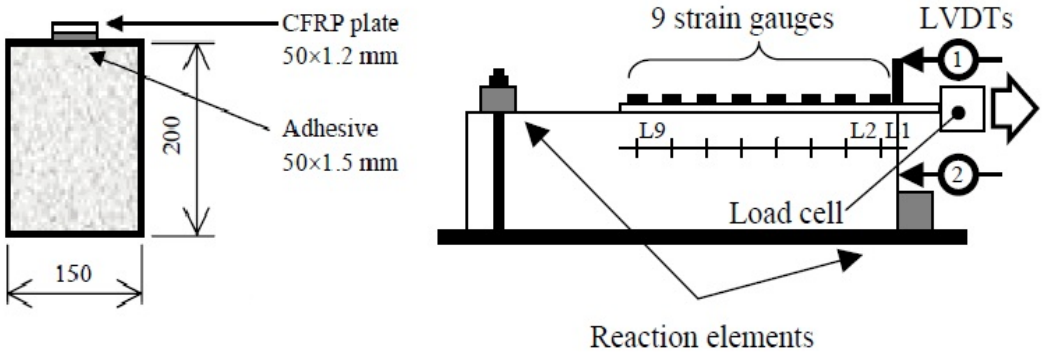

Fig 2.1 Specimen Details (Mazzotti Et Al., 2004)

Top surfaces of concrete blocks have been grinded with a stone wheel to remove the top layer of mortar, just until the aggregate was visible (approximately 1 mm). Plates have been bonded to the top surface of blocks by using a 1.5 mm thickness of two – components Sikadur-30 epoxy adhesive; curing period was at least 1 day prior to testing.

Fig 2.2 Test setup (Mazzotti et al., 2004)

From the experimental setup in Fig 2.2 we can see the concrete block was positioned on a rigid frame with two steel reaction elements to prevent horizontal and vertical translations the free end of the plate was clamped to a steel plate that was free to rotate around the vertical axis. The traction force was applied to the steel plate by using a mechanical actuator and the tests were performed under displacement control of the plate free end. A load cell has been used to record the applied traction force. Along the CFRP plate, a series of five–to–nine strain gauges (depending on the plate

length) were placed, in the centreline. Moreover, two LVDTs were placed in order to measure displacements .

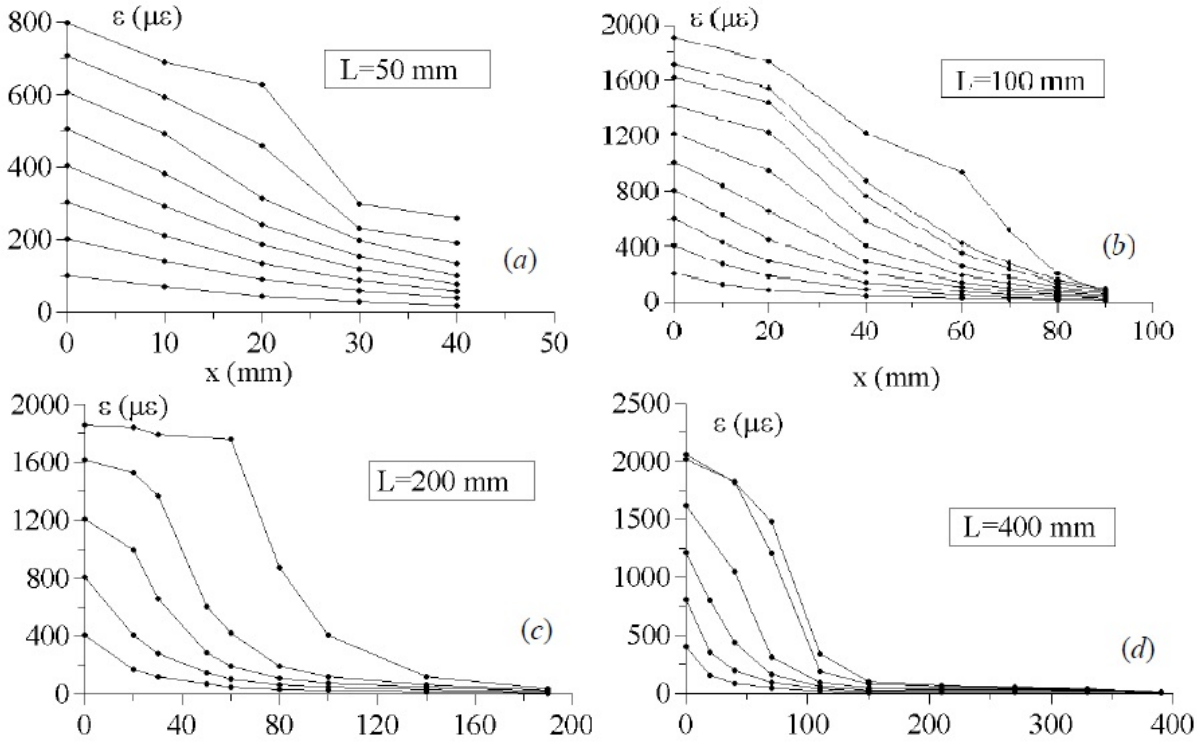

Fig 2.3 Profiles of Experimental Strains In FRP Plates Along The Bonded Lengths. (Mazzotti et al., 2004)

For the four different bonded lengths, longitudinal strains along the FRP plate at different loading levels were reported in fig 2.3 *a-d*. For bonded lengths from 100 mm to 400 mm, FRP strains are very regular for low – to – medium values of applied force, showing an exponential decay starting from the loaded section (x=0). This strain profile corresponds to a linear behavior of the interface. For high force levels, strains tend to be almost constant along FRP plate close to loaded end, due to onset of delamination phenomenon along the bonded length. where delamination has not occurred, an exponential decay behavior can be observed again.

On the contrary, for the 50 mm bonded length, an almost linear profile of strains along the anchorage has been found, also for low levels of applied force. These profiles indicate a uniform distribution of shear stresses along the anchorage. The results clearly show that the shortest bond length is significantly smaller than the effective anchorage length (the minimum length assuring maximum FRP anchoring force).

Values of FRP strains along the plate have been used to calculate the shear stress and slip distributions along the bonded lengths. Considering an elastic behavior for the composite, the average value of shear stress between two subsequent strain gauges can be written as a function of the difference of measured strains as

$$\overline{\tau}_{i+1/2} = \frac{E_p A_p \left(\varepsilon_{i+1} - \varepsilon_i\right)}{b_p \left(x_{i+1} - x_i\right)} \tag{1}$$

Where with *Ap*, being cross section of the composite. Moreover, *xi* denotes the strain gauge position and ε_i the measured strain

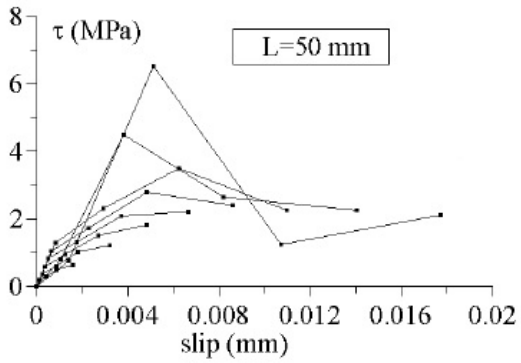

Fig 2.4 Average Shear Stress Slip Data Obtained From Post-Processing Experimental Results (Mazzotti et al., 2004)

The only exception is represented by the results from the smallest bond length case (50 mm). In this case, the length was so small that the actual slip never vanishes along the interface. Hence, the procedure adopted to obtain slips along the plate was not accurate and the researcher used calibration law for removing errors.

Nakaba et al. (2001) studied the bond behaviour between fibre- Reinforced Polymer Laminates and Concrete. To obtain the local bond stress versus slippage relationship, a double-face shear type bond test was conducted. The primary test variables are the types of fiber and concrete. The test results show that fiber stiffness influences both the bond strength and shape of stress distribution. The obtained local bond stress - slip relationships, however, are not influenced by the type of fiber. Only the maximum local bond stress increases as concrete compressive strength also increases. The

specimen details and nomenclature details are respectively explained in fig 2.5 and 2.6

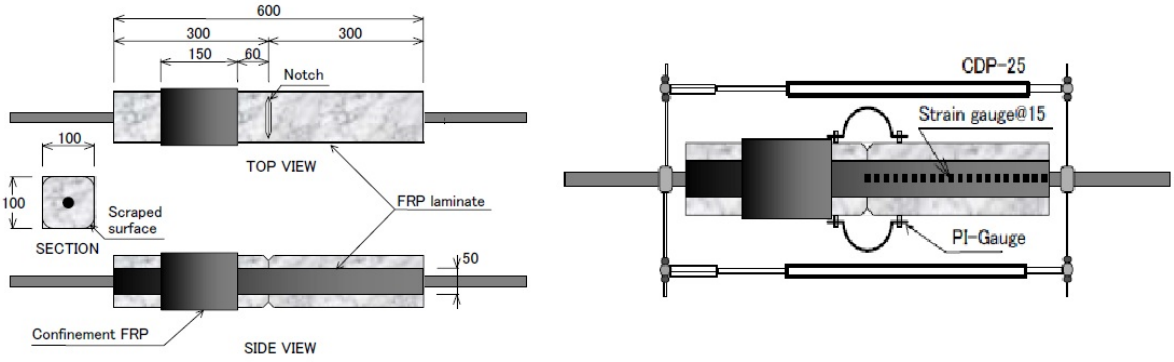

Figure 2.5 Test Specimen And Data Acquition Sketch (Nakaba et al., 2001)

To verify the influence of the quality of the substrate, the specimens were made by concrete and mortar. In addition the influence of concrete strength (50 and 24MPa) was verified.

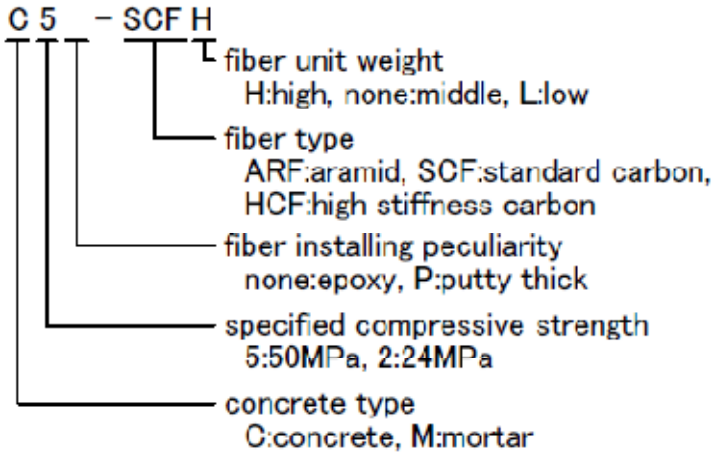

Fig. 2.6 Nomenclature of Specimens (Nakaba et al., 2001)

All the specimens were submitted to tensile force until total failure of the bond system took place. In the M5 specimens, the substrate surface on the failure face did not present many pieces of mortar bonded on the laminate

Table2.1 Properties of Mixes (Nakaba et al., 2001)

Type of Base	Compressive strength σ MPa	Splitting strength σ_t	1/3 Secant modulus E_c MPa
Concrete C5	57.6	3.25	29,000
Mortar M5-1	47.1	4.65	24,500
Mortar M5-2	50.9	4.08	25,500
Concrete C2	23.8	1.98	22,000

Table2.2 Fibre Properties (Nakaba et al., 2001)

Type of Fiber	Thickness	Unit weight	Tensile strength	Elastic modulus
	t_f ,mm	ρ,g/m^2	f_t ,MPa	E_f, MPa
Standard Carbon Fiber	0.167	150/300	4,200	2,61,100
High Stiffness Carbon Fiber	0.165	300	4,400	4,25,100
Aramid	0.193	285	2,800	1,24,500

Some pieces of concrete on the laminate could be found in the C5 specimens, and a layer of concrete was bonded on the laminate in the C2 specimens after the failure.

These facts are related to the interface between laminates and concrete, which is the region where the epoxy infiltrates into concrete and mortar, and where it is supposed to have a concentrated wearing between FRP and concrete / mortar. The layer of the interface was estimated to have approximately 1 mm for concrete surface.

Table2.3 Test Results of Specimens (Nakaba et al., 2001)

	Identification of specimen		At max. load		Ultimate		Failure mode
			Load, kN	Displacement,mm	Load kN	Displacement,mm	
C5	C5-SCFH	1	51.26	0.824	51.26	0.824	Bond failure on gauge face
		2	50.65	0.847	50.65	0.847	Bond failure on no gauge face
		3	54.48	0.998	54.48	0.998	Bond failure on no gauge face
	C5-SCF	1	37.81	1.02	37.81	1.02	Rupture
		2	33.92	1.174	30.48	1.297	Bond failure on no gauge face
		3	33.27	1.059	33.14	1.078	Bond failure on no gauge face
	C5-HCF	1	38.98	1.316	37.75	1.476	Rupture on no gauge face
		2	38.95	1.428	38.95	1.428	Bond failure on gauge face
		3	32.49	1.399	32.49	1.399	Rupture on no gauge face
	C5-ARF	1	25.52	1.764	25.52	1.813	Bond failure on no gauge face
		2	25.71	2.597	24.99	3.037	Bond failure on gauge face
		3	23.76	1.019	21.77	1.749	Bond failure on gauge face
M5	M5-SCFH	1	41.28	0.719	41.28	0.719	Bond failure on gauge face
		2	44.57	0.684	44.57	0.684	Bond failure on no gauge face
		3	47.14	0.723	46.39	0.803	Bond failure on no gauge face
	M5-SCF	1	30.7	0.958	30.49	1.529	Bond failure on no gauge face
		2	33.72	1.318	33.72	1.318	Bond failure on no gauge face
		3	32.58	1.164	32.58	1.164	Bond failure on gauge face
	M5-SCFL	1	17.51	2.14	17.5	2.14	Bond failure on gauge face
		2	17.46	2.038	16.12	2.241	Bond failure on no gauge face
		3	20.04	2.054	19.98	2.144	Bond failure on gauge face
	M5-HCF	1	33.12	1.41	33.12	1.41	Bond failure on no gauge face
		2	32.5	1.04	32.5	1.04	Bond failure on no gauge face
		3	29.28	0.715	29.28	0.715	Bond failure on no gauge face
	M5-ARF	1	25.71	2.597	25.14	2.665	Bond failure on gauge face
		2	24.35	2.256	23.96	2.297	Bond failure on no gauge face
		3	25.42	1.752	23.4	2.01	Bond failure on no gauge face
C2	C2-SCF	1	28.18	1.369	27.82	1.644	Bond failure on no gauge face
		2	27.74	1.343	25.62	1.606	Bond failure on gauge face
		3	30.17	1.8	29.89	2.806	Bond failure on gauge face
	C2P-SCF	1	29.08	1.479	28.43	1.512	Bond failure on no gauge face
		2	30.28	1.569	29.57	1.616	Bond failure on gauge face
		3	30.58	1.046	25.24	1.718	Bond failure on no gauge face

In this a local bond sress model was proposed based on Popovics's equation, which represents with good accuracy the experimental results. The model was also verified by comparing the test results from a previous study with the analytical results obtained with the present model. Additionally, the effective bond length for each combination of FRP – concrete / mortar was presented

1. The maximum load increases as the stiffness of FRP also increases;

2. Putty thickness is shown to have no effect, and the in- cremental increase of its layer did not imply an increase in maximum load; and

3. Maximum local bond stress is not influenced by the type of FRP, but increases as concrete compressive strength increases.

Lorenzis et al. (2001) discussed Bond of fiber-reinforced polymer laminates to concrete. In this paper, flexural test specimens were prepared to address some of the factors expected to affect bond like bonded length, concrete strength, number of plies (stiffness), ply width, and, to a limited extent, surface preparation.

The specimen used for this project was a plain concrete beam with an inverted-T shape, as shown in Fig.2.7. The beam was simply supported, with a span of 1067 mm and a total length of 1219 mm. A steel hinge at the top and a saw cut at the bottom, both located at midspan, were used to control the distribution of the internal forces. During loading, the saw cut caused a crack to develop at the center of the beam and extend up to the hinge. Therefore, the compressive force in the beam at midspan was located at the center of the hinge and the internal moment arm was known and constant for any given load level above the stabilized cracking load.

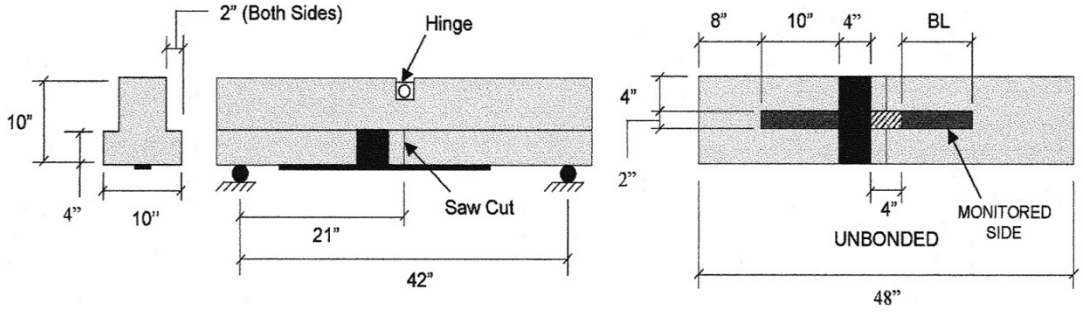

Fig2.7 Test Specimen (Lorenzis et al. 2001)

A 2 in. (51 mm) wide CFRP strip was bonded to the tension face of the beam. A transverse sheet was placed on one side to force failure to occur at the other end. In addition, the sheet was left unbonded for approximately 2 in. (51 mm) on each side of midspan. The design choices were made to ensure that no cracking would occur within the bonded area. Three series of specimens were tested. Each series consisted of six specimens with three different bonded lengths. Either the concrete strength or the number of plies of CFRP was varied between each series. Description of the specimens is reported in Table 2.4**.**

Table2.4 Specimen Nomenclature and Properties in the Test

(Lorenzis et al., 2001)

Series no.	Specimen code	Concrete Compressive strength, psi	No. of plies	Bonded length, in.	Ultimate tensile load in FRP, lb	Ultimate stress in FRP, ksi
I	6-1-4-1	6860	1	4	3720	286
	6-1-4-2				3990	307
	6-1-8-1			8	3560	274
	6-1-8-2				3190	245
	6-1-12-1			12	3830	295
	6-1-12-2				3390	261
II	6-2-4-1	5900	2	4	5930	228
	6-2-4-2				5140	198
	6-2-8-1			8	4630	178
	6-2-8-2				6290	241
	6-2-12-1			12	5590	215
	6-2-12-2				5080	195
III	3-1-4-1	3550	1	4	3300	254
	3-1-4-2				3120	240
	3-1-8-1			8	4450	342
	3-1-8-2				2920	225
	3-1-12-1			12	4770	367
	3-1-12-2				3450	265

After the beams had cured for 10 to 14 days, the concrete surface on which the CFRP had to be applied was sandblasted to remove the top layer of mortar until the aggregate was visible. The approximate depth of sandblasting was 1.5 mm. A composite system including a unidirectional fiber prepreg CFRP sheet, primer, and saturant was used for this experimental program. The sheet had an ultimate tensile strength of 4272 MPa, a design tensile strength of 3790 MPa , a modulus of elasticity of 227 GPa and a fiber thickness of 0.16 mm, The resin was allowed to cure for at least 7 days prior to testing. The thickness of each layer of the composite system was determined by using a scanning electron microscope (SEM). The resulting thicknesses were: 0.43, 0.94, and 0.16 mm for the primer, first resin layer, and CFRP sheet, respectively. After the testing of the three series of specimens was complete, three more specimens were tested. Two specimens were made with 102 mm wide CFRP

sheets instead of 2 in. 51 mm sheets. This was to determine whether the width of the sheet had an effect on the strain distribution. The bonded lengths of the specimens were 203 and 305 mm, while the nominal concrete strength was 41.3 MPa. These specimens were instrumented similarly to those of the first three series. Finally, one specimen was tested wherein the surface preparation was changed. The surface was roughened by adding notches using a hammer and chisel. This specimen had a 305 mm bonded length and 41.3 MPa nominal concrete strength. The purpose of this test was to determine if surface preparation affected the average bond strength. No strain gages were used in this test because the main interest was to see if the ultimate load was increased by the different surface preparation.

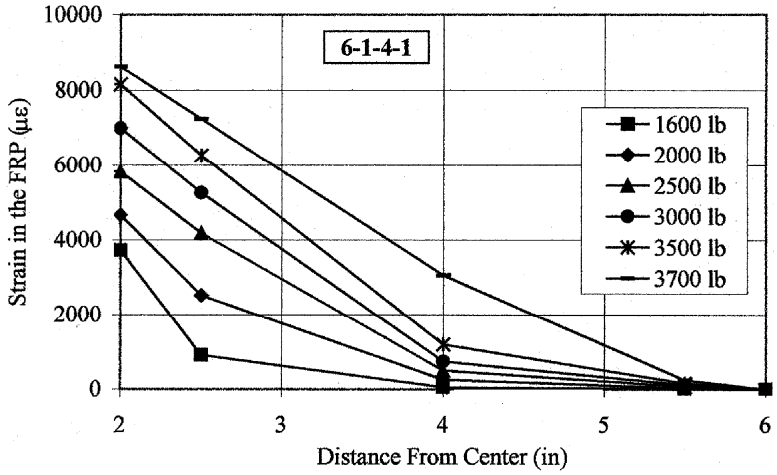

Fig 2.8 Strain-Versus-location Diagram of Specimen 6-1-4-1. (Lorenzis et al., 2001) (Note: 1 in. = 25.4 mm; and 1 lb = 4.45 N.)

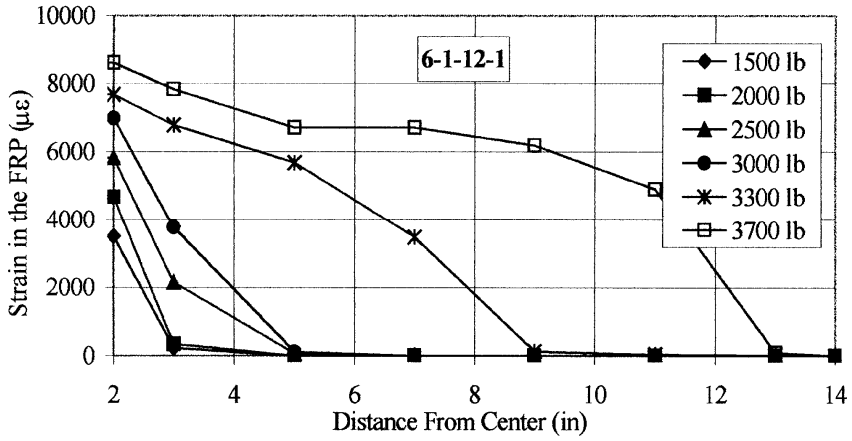

Fig 2.9 Strain-versus-location Diagram of Specimen 6-1-12-1. (Lorenzis et al., 2001)

(Note: 1 in. = 25.4 mm; and 1 lb = 4.45 N.)

Data collected from the strain gages were used to develop strain distribution curves. A typical strain-location graph for the 102 mm bonded length can be seen in **Fig. 2.8** while Fig. 2.9 shows a typical graph for the longer bonded lengths. By comparing these figures, it can be seen that, at early stages of loading, the curves show the same behavior. They both have a nonlinear shape, and the strain gages far from the center do not read strain. Also, as the load increases, the curves tend to attain a linear shape. It can be assumed that joint failure begins immediately after the point when the curve becomes linear. This corresponds to the attainment of a uniform bond stress along the portion of laminate that is taking the load. The length of this portion is what has been previously indicated as effective bond length. Once failure begins, the behavior in the two cases is different. The specimens with the 4 in. (102 mm) bonded length fail suddenly. For the 8 and 12 in. (203 and 305 mm) bonded lengths, failure occurs in stages due to the longer. bonded length.

This progressive failure is indicated by the strain distribution. The strain becomes almost constant at the beginning of the bonded length, which means that no load is transferred into the concrete in that portion of the bond because the joint has begun to fail. In other words, the effective length of the CFRP sheet takes the entire load to a certain point at which localized joint failure occurs, causing the effective bond length to shift. This shifting continues until the CFRP sheet has completely peeled from the concrete. Visual inspection of the specimens after the test revealed that failure occurred in the concrete-adhesive interface with very little or no sign of damage in the concrete surface. When comparing results, it was found that the bonded length did not affect the bond failure load. It was concluded that an effective length exists beyond which no stress is transferred until peeling occurs.

While it was expected that the concrete strength would have an effect on the bond strength, there was no evidence from this investigation. Because failure occurred at the concrete-epoxy interface, the concrete strength did not affect the ultimate load. The number of plies used to make the CFRP laminate affects the bond failure load. For two plies of CFRP sheet to be as efficient as one ply, however the ultimate load would have to double. As expected, this does not occur. The average of the ultimate loads of Series II is only 1.5 times that of Series I. Two specimens with a 4 in. (102 mm) sheet width were also tested to verify that the width of the CFRP sheet does not affect the bond strength. The two specimens with 8 and 12 in. (203 and 305 mm) bonded length failed at a load 35.09 and 35.54 kN, respectively. These ultimate loads

are approximately twice those of the specimens with same bonded length and 2 in. (51 mm) wide sheets. Also, the failure mode and strain distribution were the same. Hence, it was concluded that the width of the sheet did not influence the bond strength. This is contrary to findings of other researchers (Brosens and Van Gemert 1999; Ueda, Sato, and Asano 1999) who observed an increase in the average bond strength with decreasing sheet width. The contradiction is simply explained with the different failure mode: when delamination occurs by shearing of the superficial concrete layer attached to the FRP, the fracture zone is generally wider than the laminate, and the ratio of its area to the bonded area becomes larger as the laminate width decreases. This size effect is not present when the bond failure crack propagates in the adhesive or at the concrete-adhesive interface.

Finally, the performance of the specimen whose surface had been roughened by chiseling was much better than that of the specimen with sandblasted surface. The former failed at a load level of 5590 lb (24.86 kN), as opposed to 3830 and 3390 lb (17.04 and 15.08 kN) of Specimens 6-1-12-1 and 6-1-12-2, respectively. CFRP rupture was attained with the chiselled surface. The sheet began peeling until it reached the location of the first set of notches. The notches seemed to anchor the sheet to the concrete. This result seems to confirm that the surface preparation of the concrete can significantly affect the average bond strength.

Taranu et al. (2011) studied the bond between CFRP plates and concrete. In this matter an experimental investigation was carried out aiming to determine an appropriate assessment of the interfacial region. For the experimental program a single batch of concrete blocks with dimensions of 150 × 150 × 400 mm were casted from a concrete mix having a maximum aggregate size of 16 mm. The proposed test set-up is shown schematically in Fig 2.10 , and detailed drawings of the instrumentation and positioning of the LVDTs and strain gages are illustrated in Fig. 2.11. The relative displacements between CFRP reinforcing laminates and concrete were recorded with LVDTs placed on each monitored side, at the location of the transition between the central un-bonded and the bonded zone. Whereas, five strain gages were applied directly on the FRP reinforcement at 10, 80, 150, 220 and 290 mm from the end of the concrete prism.

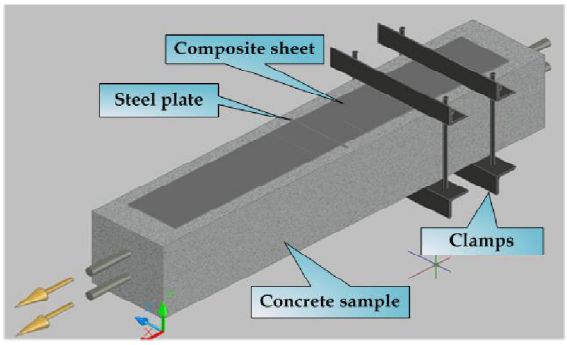

Fig 2.10 Test Specimen (Taranu et al., 2011)

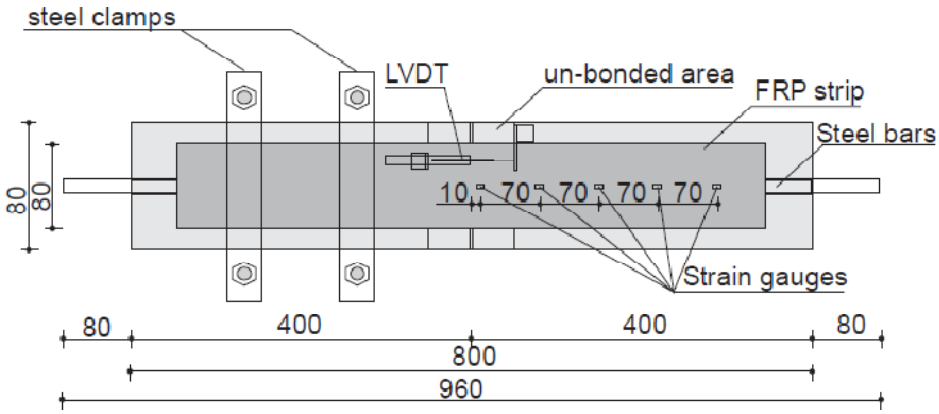

Fig 2.11 Specimen Instruementation (Taranu et al., 2011)

Tests were carried out using a universal testing machine of 3,000 kN. The rate of loading (displacement rate or load rate) is preferred to be constant during the test. A displacement rate of 0.1 mm/min or a loading rate of 6 kN/min was proposed.

The double shear tests that have been performed on the prepared specimens are marked as follows: C1 for Sika Carbodur S1012, C2 for Sika Carbodur M1014 and C3 for CFK 150/2000 bonded plates. Tests were performed on three specimens of the same type, using an epoxy adhesive, namely Sikadur 30. The average experimental results obtained for each set of specimens in terms of maximum load (N_{fa},max), ultimate strength (σu), tensile factor ($\sigma u/ff$), ultimate strain (εu) and maximum slip recorded by LVDTs (sLVDT) are summarized in Table 2.5

Table 2.5 Test results of specimen (Taranu et al., 2011)

Specimen	C1	C2	C3
N_{fa},max , [kN]	46.2	57.8	57.15
σ_u , [MPa]	385.2	412.96	476.25
σ_u/ff , [MPa]	12.43	13.32	–
εu , [%]	0.124	0.12	0.138
LVDT , [mm]	0.16	0.24	0.49

Debonding of the CFRP sheets from the concrete surface represents the most common failure mode The failure was initiated due to shearing of the concrete just beneath the adhesive layer. Beacause shear strength of concrete is proportional to tensile strength, the value of the ultimate bond strength will be proportional to tensile strength. Failure had a brittle manner, typical for concrete specimens with laterally attached CFRP bonded sheets.

Fig 2.12 Typical Failure Mode. (Taranu et al., 2011)

From the measured strain profiles along the joint, it is possible to compute the mean shear stress distribution Given two consecutive strain readings, εi and $\varepsilon i+1$, at positions i and $i + 1$, the laminate thickness, tf , its modulus of elasticity, Ef, and the distance, Δxi , between the considered gages, one can determinate the average shear stress, $\tau(x)$, between two consecutive strain gages as follows:

$$\tau(x) = Ef * tf * \frac{\Delta \varepsilon i}{\Delta xi}$$

Through the integration of the strain along the bonded length one can compute the slip between CFRP reinforcement and concrete. On the basis of strain compatibility in the infinitesimal range, d*x*, of the CFRP–concrete interface, and neglecting the concrete strain, the following equation can be written:

$$s(x) = s(0) + \int_0^{Lb} \varepsilon f * dx$$

where $s(x)$ is the slip along the bong length, $s(0)$ – the slip at the loaded end, εf – the strain in the CFRP reinforcement. The comparison between specimens reinforced with different CFRP plates, in terms of bond stress *versus* slip, is reported in Fig. 8. All curves are characterized by a linear behavior.

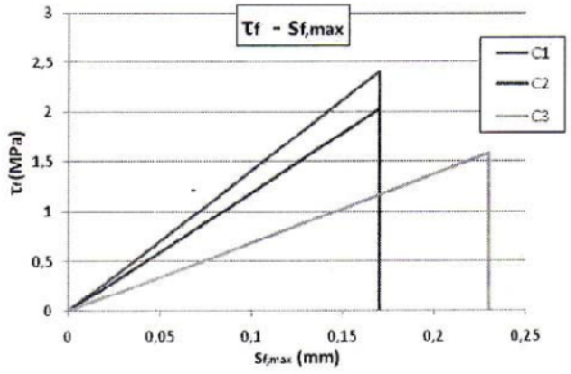

Fig. 2.13 Bond *vs*. Slip Diagram (Taranu et al., 2011)

The failure at the interface occurred in the substrate and had a brittle manner. Therefore it can be stated that the shear strength capacity of the substrate material is a major parameter of the interface region behaviour.

Mazzotti et al. (2008) A new single-shear set-up for stable debonding of FRP–concrete joints. Allowing for a stable debonding process, Method was adopted to perform FRP–concrete bond tests. The specimen back side was fixed to an external retaining system, i.e., both concrete and FRP reinforcement are clamped at their end section. During the test, a very stable debonding process occurred at constant applied force, corresponding to the debonding force of an anchorage of infinite length. FRP–concrete bonding has been investigated by testing a number of specimens with CFRP reinforcement bonded to concrete prisms.

Load was applied at one end of the plate, whereas the opposite extremities of both reinforcement and concrete specimen are clamped to an external retaining system. Concrete block dimensions are 150 *200 *600 mm. They have been fabricated using normal strength concrete. Five 15 *30 cm standard cylinders have been also poured and used to evaluate mechanical properties of concrete.

As for the composites both, CFRP sheets and plates have been used. For specimens P5, P8, CFRP sheets were adopted: one layer of Sika Wrap Hex 230 C, 80 mm wide (bp) and 0.13 mm thick (hp). For specimens P1, P6, P9, Sika CarboDur S plates have been glued to concrete, 80 mmwide and 1.2 mm thick

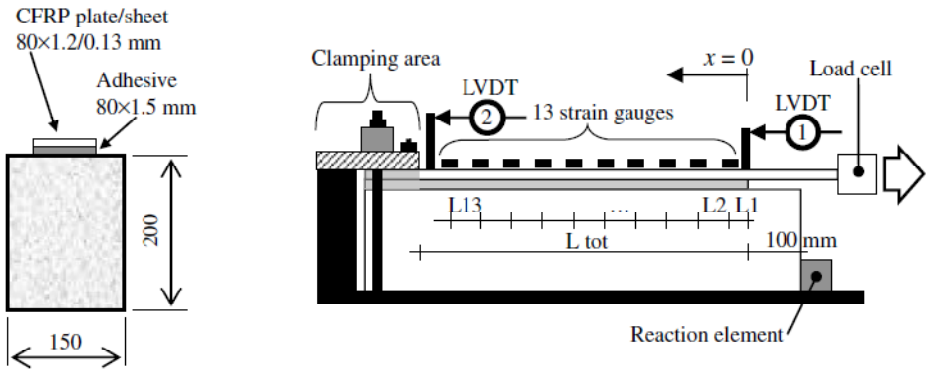

Fig. 2.14 Experimental Set-Up: (a) Specimen Transverse Section; (b) Side View with Instrument Position and Clamping System for Both Concrete Specimen and CFRP Plate (Mazzotti et al., 2008)

Three different techniques for surface preparation have been adopted in order to study its effect on debonding force and fracture energy of the interface law:

1. Sand blasting: Concrete surfaces have been sand blasted in order to remove the layer of mortar over the aggregates, so obtaining a very rough (and slightly damaged) concrete surface (specimens P5A, P5B with FRP sheets and P9A, P9B with FRP plates).

2. Type 1 grinding: Surfaces of concrete blocks have been grinded with a stone wheel to remove the top layer of mortar, just until the aggregate was visible (approximately 1 mm); due to the very small dimension of the marble powder glued to the wheel, concrete surface was very smooth (specimens P8A, P8B with FRP sheets and P1A, P1B with FRP plates). Type 2 grinding: Top surfaces have been grinded by using a

different stone wheel, with a coarse iron powder, so providing for a rough and apparently not damaged concrete surface (specimens P6A, P6B with FRP plates).

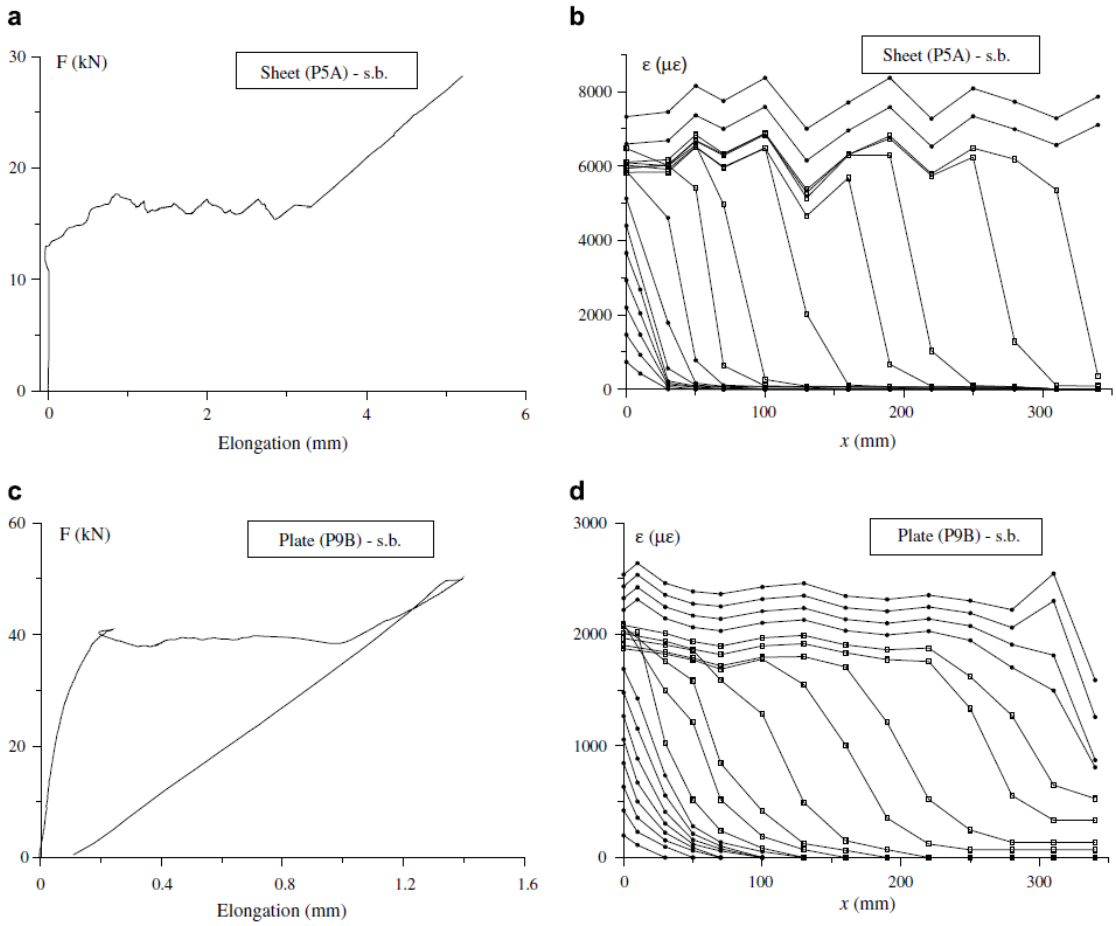

Fig. 2.15 Results From Delamination Tests on FRP Sheets and Plates Bonded to Concrete (Mazzotti et al., 2008)

(a, c) force–plate elongation curves, (b, d) strains along the FRP reinforcement at different levels of applied force, before and during debonding; measures during debonding phase.

The results obtained for CFRP sheet and plate bonded to concrete surface previously subject to sand blasting treatment are reported (specimens P5A, P9A, respectively). Force–CFRP elongation curves of two specimens are reported in fig 2.15. a and c. In both cases, three main behaviours can be identified: the first branch is almost linear up to 70–80% of maximum transmissible force. Beyond that value, stiffness degradation can be observed due to the onset of debonding, occurring when shear strength is attained at the beginning of the bonding length. The subsequent debonding occurs at an almost constant value of applied force. Duration of debonding process

during the tests has been 15–30 s. Finally, after complete debonding, the only load-carrying element is the CFRP reinforcement, properly fixed at the opposite extremity, whose behaviour is linear elastic.

Some analogies with the tension-stiffening effect can be drawn. Prior to debonding, the specimen is in an uncraked state (usually defined as State I, where both concrete and reinforcement contribute to specimen stiffness). After complete debonding, only CFRP carries the applied load (State II); the debonding process links these two limit states. In all tests we have seen the debonding failure occurred inside the concrete hence leaving a variable (small) quantity of it attached to the adhesive glued to the FRP element.

Table 2.6 Test Results of Specimen (Mazzotti et al., 2008)

Type	Specimen	Fmax (kN)	Fmax-mean (kN)	E_p (MPa)	G_f (MPa mm)
Sheet – sand blasting	P5A	16.5	16.95	283	653 0.61
	P5B	17.4			
Sheet – Type 1 grinding	P8A	14.4	14.5	2,91,024	0.43
	P8B	14.6			
Plate – sand blasting	P9A	37.6	38.35	197,630	0.49
Plate – Type 1 grinding	P1A	34.5	34	1,95,700	0.39
	P1B	33.5			
Plate – Type 2 grinding	P6A	41	39.5	1,95,460	0.52
	P6B	38			

In the Table 2.6, the values of modulus of elasticity of plates and sheets, obtained from tests by applying couples of strain gauges in the unbonded portion of FRP reinforcement, are also reported. It is worth noting that, if sand blasting is used to remove the top layer of mortar on concrete surface, the debonding force is greater than grinding the surface with a stone wheel (Type 1 grinding), 15% and 12% for FRP sheets and plates, respectively. In fact, epoxy resin penetration inside the external layer of concrete is improved by sand blasting providing for better performances, even if the concrete surface is slightly damaged. This is confirmed by comparison of fracture surfaces after debonding for different surface preparation: grinding or alternatively sand blasting. In the first case, a very thin layer of concrete is attached to the adhesive-plate debonded system, and in some portions there is no concrete at all.

In the second case (sand blasting), the characteristic inclined cracks on the concrete surface are evident, and a significantly thicker and rough layer of concrete is attached to the adhesive.

Rebecca et al (2012) studied the bond and force transfer of FRP Materials bonded to Concrete Using sitecure System. Sitecure is an innovative processing system in which vacuum and heat is applied to pre-preglaminates in order to achieve high quality of bond. Prepreg laminates contain some amount of matrix to bond the fibres to each other. Use of vacuum and heat aims to improve the long term durability and fatigue performance of the bond line and achieve faster curing on-site for enclosing large structures. The most important advantage of this technique using pre-pregs is the ability to achieve a higher transition temperature (Tg) for the resin. The properties of FRP decrease when it experiences temperatures higher than Tg.

13 concrete prisms, 150mm in width 150mm in depth and 300mm in length were casted. To investigate the applicability of the Sitecure technique against conventional strengthening systems, the performance of the sitecure technique on FRP bonded concrete prisms was compared to wet lay-up and pultruded carbon FRP plates. The dimensions of the FRP plates were 75mm in width and 200 mm in length.

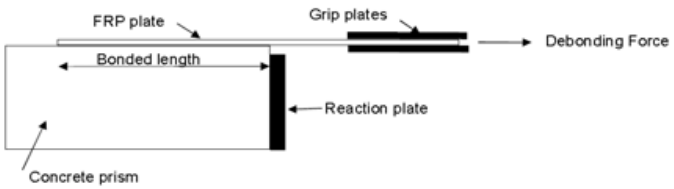

(a)

(b)

Fig2.16 (A) Schematic View of Specimens And (B) Picture of Test Set Up. (Mazzotti et al., 2008)

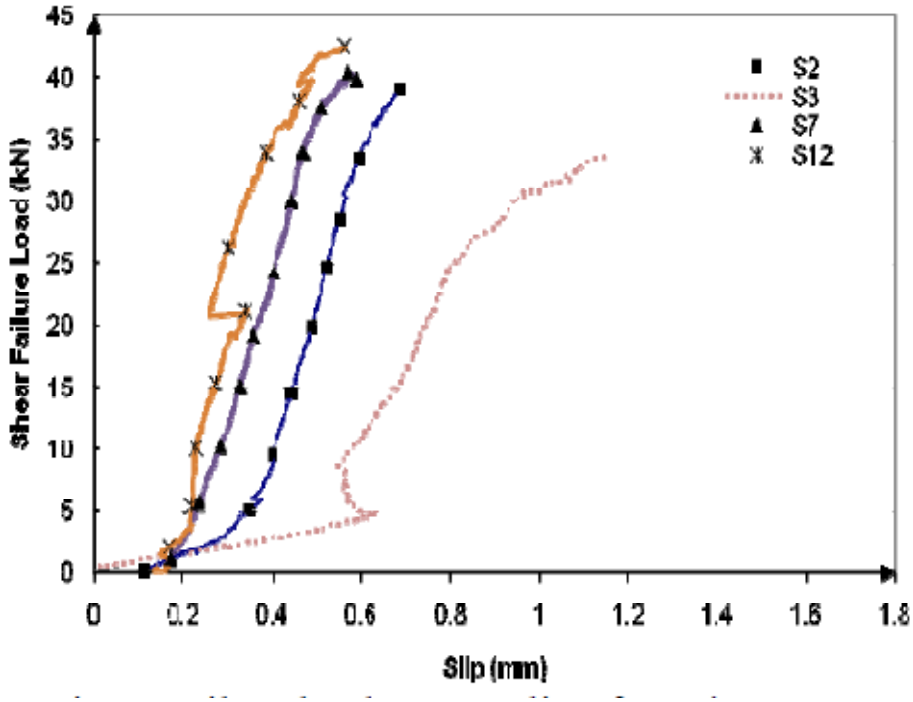

Fig 2.17 Failure Load Versus Slip of Wet Lay-up, Pultrusion and Sitecure Systems. (Mazzotti et al., 2008)

It can be seen from fig 2.16 that the load carrying capacity of samples using the Sitecure technique to bond FRP materials on the concrete substrate, increased significantly in comparison with the two other systems. For all of the samples when the maximum shear load was reached, a longitudinal crack was propagated in the interfacial element between FRP and concrete and detaching of FRP coincided with a high sound. Therefore, the load carrying capacity dropped suddenly. The wet lay-up system showed the lowest maximum load capacity between retrofitting techniques. In the wet lay-up system, the quality of applied fibre reinforced polymer depends highly on the skill of workers and can be varied from one sample to the other. However, in Sitecured specimens the quality of the FRP is controlled since the application of the prepreg laminate was applied via vacuum and cured under heat.

Wan et al (2002) studied the experimental investigation of bond between FRP and concrete modified double cantilever beam specimens were used to investigate the fracture behavior of the bond region between FRP and concrete. Crack growth and crack opening displacement were acquired through a computer vision system and image analysis software. Based on experimental observations, the following conclusions are attained: A photograph of the camera system and test setup used in

this work to measure COD. The digital camera was mounted on a three-dimensional translation stage so that the camera can be translated with the crack tip region and images of the crack-tip region acquired during the stable tearing process.

COD is directly related to the percentage of concrete on the fracture surface; COD increases correspondingly with the increasing of concrete percentage. COD is nearly constant with a mean of 0.033 mm and a standard deviation of 0.003 mm when the percentage of concrete is greater than 50% and a transition region of substantial variability exists when the percentage of concrete is between 10% and 50% of the fracture surface. Thus, the critical COD is a minimum when the crack grows within the FRP concrete interface (concrete percentage is less than 10%). Similarly, the critical COD is a maximum when at least 50% of the fracture surface is within the concrete. The measured values for mixed mode Crack Opening Distance (COD) indicate that the flaw is growing in predominantly mode I conditions, with a small component of mode II COD remaining constant throughout the growth process. The measured values for mixed mode COD and G are related to the percentage of concrete on the fracture surface; increasing as the percentage of concrete on the fracture surface increases. The behavior suggests threshold values of COD may be expressed as a function of the percentage of concrete on the fracture surface.

Mostofinejad et al (2012) studied the externally bonded reinforcement in grooves (EBRIG) technique to postpone debonding of FRP sheets in strengthened concrete beams. Recently a new method for flexural strengthening of concrete beams with FRP sheets, named as grooving method (GM) with the special technique of externally bonded reinforcement on grooves (EBROG), was introduced as alternative to conventional externally bonded reinforcement (EBR). For this purpose, 32 beam specimens with dimensions of 120*140* 1000 mm were casted and was strengthened with one, two or three layers of FRP sheets and then subjected to four-point flexural loading.

Results showed considerable increase in ultimate limits for beams strengthened with EBROG and EBRIG techniques compared to those strengthened with EBR method. The EBRIG technique performed as good as EBROG for one layer of strengthening FRP sheet; however, it permitted for higher failure loads and displacements compared

to EBROG method when multiple-layer FRP sheets were usedThis technique is named externally bonded reinforcement in grooves (EBRIG).

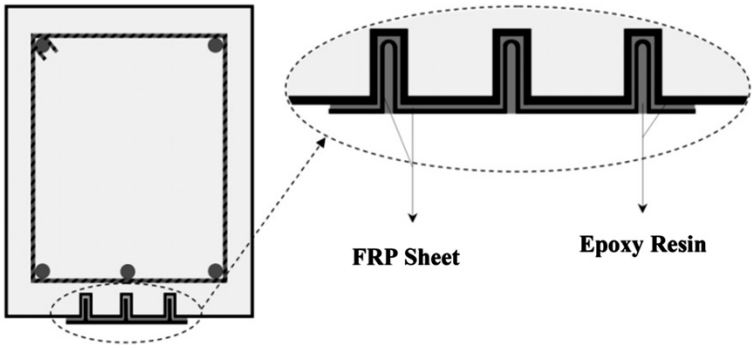

Fig 2.18 Externally Bonded Reinforcement in Grooves (EBRIG) Technique. (Mostofinejad et al.,2012)

The beams were with length of L = 1000 mm, width of b = 120 mm and height of h = 140 mm. In order to ensure bending failure modes for all the beams and to prevent any undesired shear failure during the tests, all the specimens were internally reinforced with 5 mm diameter steel stirrups fixed with appropriate spacers and wires. two linear variable differential transducers (LVDTs), mounted at the mid-span, were installed and connected to a data logger to obtain an accurate force and deflection reading. Crack initiation and propagation were also monitored by visual inspection during the tests.

The variables examined in the experimental program were as follows:

(1) The strengthening technique: Four distinct strengthening methods, i.e. EBR, NSM, EBROG and EBRIG were examined. A group of specimens were also considered in which FRP sheets were applied to the beams using EBR technique without any surface preparation.

(2) Number of bonded FRP sheets: All of the strengthening methods were experimented for one, two and three layers of FRP sheets.

In addition, each test was applied to two identical beams in order to avoid any undesired mistake and ensure test repeatability; therefore, flexural tests were conducted on six groups

The first group consisted of two control beams without strengthening; while the beams in the second group were strengthened with EBR method but without any surface preparation (WSP group). The third group consisted of six beams strengthened with EBR method with conventional surface preparation. In this group, first, a thin layer of concrete was removed. Then the surface was cleaned with jet air and finished with Sikadur C31 as primer. Then a layer of epoxy (Sikadur C300) was applied and followed with the wet application of FRP sheets, The fourth group was included of six specimens which were strengthened with NSM technique. In this set of beams in order to make it possible for comparison with other groups, unconventionally carbon fibers were embedded into the craved grooves and the grooves were filled with epoxy resin Sikadur C300. The beam specimens in the fifth group were strengthened with EBROG method. The strengthening technique consisted of the following steps:

(a) Three grooves of about 850 mmlong, 7 mmwide and 10 mm deep were cut in the concrete cover of the tension face of the beam.

(b) The grooves were cleaned with compressed air and filled with epoxy Sikadur C31.

(c) A layer of epoxy Sikadur C300 was applied on the surface of the beams.

(d) Carbon fiber sheets were cleaned and adhered to the surface.

(e) The epoxy in excess was removed.

Table 2.7 Details of Tested Specimen (Mostofinejad et al., 2012)

Details of tested specimens.

(1) Beams	(2) Number of FRP layers	(3) Cylindrical compressive strength (MPa)	(4) Average ultimate load (kN)	(5) Average ultimate displacement (mm)	(6) Increase in ultimate load (%) compared to: WSP specimens	(7) Increase in ultimate load (%) compared to: Reference beam	(8) Failure mode
Reference beam							
RB	0	34.8	6.8	0.4	–	–	Flexural failure
Without surface preparation							
WSP-1L	1	37.6	8.4	3	–	23	Plate-end interfacial debonding
WSP-2L	2	38.4	14.3	1.9	–	110	Plate-end interfacial debonding
WSP-3L	3	36.8	20.6	2.6	–	202	Plate-end interfacial debonding
Externally bonded reinforcement (EBR)							
EBR-1L	1	36.7	9.2	2.8	10	35	Plate-end interfacial debonding
EBR-2L	2	37.1	14.5	2.7	1	113	Plate-end interfacial debonding
EBR-3L	3	35.9	22.7	3.3	10	234	Plate-end interfacial debonding
Near surface mounted (NSM)							
NSM-1L	1	35.3	18.6	6.7	121	174	FRP rupture
NSM-2L	2	33.9	27.5	7.2	92	304	FRP debonding
NSM-3L	3	34.2	35	5.7	70	414	FRP debonding
Externally bonded reinforcement on grooves (EBROG)							
EBROG-1L	1	37.2	20	6.1	139	194	FRP rupture
EBROG-2L	2	37.8	35.5	7	148	422	Plate-end interfacial debonding
EBROG-3L	3	36.8	41	7	99	502	Plate-end interfacial debonding
Externally bonded reinforcement in grooves (EBRIG)							
EBRIG-1L	1	37	20.3	6.7	142	198	FRP rupture
EBRIG-2L	2	37.8	40.9	8.2	186	501	Concrete cover separation
EBRIG-3L	3	36.3	52.5	9.7	155	672	Concrete cover separation

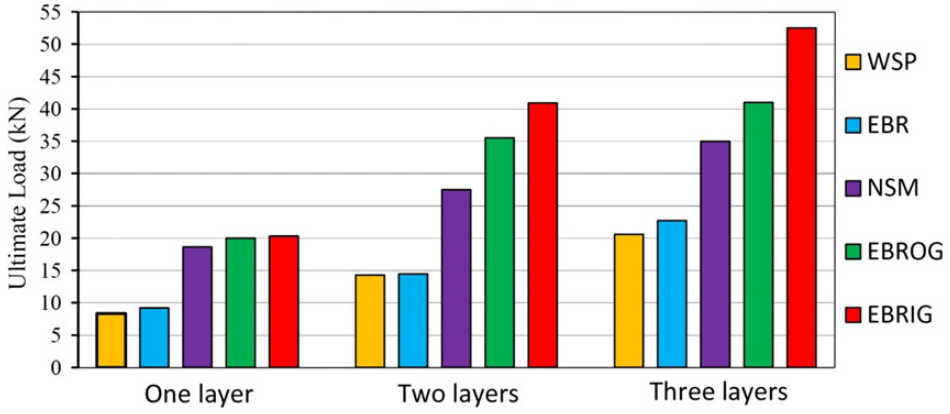

Fig2.19 Comparison Between The Ultimate Loads of Specimens with Different Methods of Strengthening. (Mostofinejad et al., 2012)

From the results we can see that the ultimate loads of the strengthened beams have been compared with those of the same beams strengthened without surface preparation. It can be observed in the table that the maximum load capacity of the EBR-1L has increased 10% compared to that of WSP-1L. This increase is respectively 121%, 139% and 142% for NSM-1L, EBROG-1L and EBRIG-1L

specimens. When specimens are strengthened with two layers of FRP sheets, the increase in ultimate load compared to that of WSP-2L is 1%, 92%, 148% and 186% for EBR-2L, NSM-2L, EBROG- 2L and EBRIG-2L specimens, respectively. In addition, for the test beams strengthened with three layers of FRP sheets, the increase in ultimate loads compared to that of WSP-3L specimen is 10%, 70%, 99% and 155% for EBR-3L, NSM-3L, EBROG-3L and EBRIG-3L specimens, respectively.

In Fig. 2.19, a comparison has been made for the ultimate loads of all the specimens, showing the significant influence of different strengthening techniques on the ultimate load carrying capacity of the beams. In fact, due to better performance of NSM, EBROG and EBRIG methods in transferring the therefore considerably increase the stiffness and ultimate load of the beams compared to uni-layer strengthening FRP.

In column 7 of Table 2.7, the ultimate load of each test beam has been compared with that of the reference beam without any flexural strengthening. It is seen in the table that for WSP-1L, EBR-1L, NSM-1L, EBROG- 1L and EBRIG-1L specimens, the increases are 23%, 35%, 174%, 194% and 198%, respectively. For WSP-2L, EBR-2L, NSM-2L, EBROG-2L and EBRIG-2L specimens the increases in ultimate loads are 110%, 113%, 304%, 422% and 501%, respectively. It is also seen that for WSP-3L, EBR-3L, NSM-3L, EBROG-3L and EBRIG-3L specimens, the increases are respectively 202%, 234%, 414%, 502% and 672%.

Hence from the above results it was found that Surface preparation can increase the ultimate load capacity of strengthened beams compared to those lacking any surface preparation. These increases were 10%, 1% and 10% for the beams strengthened with one, two and three layers of FRP sheets, respectively.

Cutting longitudinal grooves and filling them with an appropriate epoxy in EBROG method is an effective substitute for surface preparation, and can cause a great increase in ultimate load of beams compared to those without any surface preparation. In this research, these increases were respectively 139%, 148% and 99% for the beams with one, two and three layers of FRP.

By cutting longitudinal grooves and adhering FRP layers directly to the grooves surfaces in EBRIG method, the contact area between FRP and strong concrete layer is increased. Therefore, considerably higher failure loads can be achieved compared to

other strengthening techniques. In this study, 142%, 186% and 155% of increase in ultimate load were achieved respectively for the beam specimens strengthened with one, two and three FRP layers using EBRIG technique compared to those without any surface preparation.

CHAPTER 3 EXPERIMENTAL SETUP

3.1 INTRODUCTION

The aim of the experiment is to compare different surface preparation and to study the debonding mechanism. The brief description all materials and equipments required to perform tests is discussed in this chapter. Furthermore different surface preparation and experimental program is discussed in the end.

3.2 MATERIALS AND EQUIPMENTS

For the entire experimental programme the following materials and equipments are used.

3.2.1 Cement

Cement is a fine, grey powder. It is mixed with water and materials such as sand, gravel, and crushed stone to make concrete. The cement and water form a paste that binds the other materials together as the concrete hardens. Grade 53 Ultra Tech cement is used for casting beams. The cement was of uniform colour i.e. grey with a light greenish shade and was free from any hard lumps. The tests are conducted on the cement before its use and the results are

Table 3.1 Properties of Cement

Sr. No.	characterstics	Test value	Value specified by IS :1489-1991 (Part 1)
1	Standard Consistency (%)	32	--------
2	Setting time (minutes)		
	1.Initial	105	30 (min)
	2.Final	255	600 (max)
3	Specific gravity	3.1	-------
4	Compressive strength		
	7 days(MPa)	27	22 (min)
	28 days(Mpa)	39	33 (min)

3.2.2 Aggregates

Aggregates are the collection of items that are gathered together to form a total quantity. This includes sand, gravel, crushed stone, slag, or recycled crushed concrete. The aggregates generally used are of following two types:

3.2.3 Coarse Aggregates

The material which is retained on IS sieve no. 4.75 is termed as a coarse aggregate. The crushed stone is generally used as a coarse aggregate. The nature of work decides the maximum size of the coarse aggregate. The aggregates were washed to remove dust and dirt and were dried to surface dry condition. The aggregates were tested as per IS: 383-1970. The results of various tests conducted on coarse aggregate are given in Table 3.2 and Table 3.3 shows the sieve analysis results.

Table 3.2 Properties of Coarse Aggregates

Sr.no	Characterstics	nominal size	
		20 mm	10 mm
1	Specific gravity	2.6	2.66
2	Total water absorption(%)	1.9	1.87
3	fineness modulus	6.87	6.36

3.2.4 Fine Aggregates

The sand used for the experimental programme was locally procured and conformed to Indian Standard Specifications IS: 383-1970. The sand was first sieved through 4.75 mm sieve to remove any particles greater than 4.75 mm and then was washed to remove the dust. Properties of the fine aggregate used in the experimental work are tabulated in Table 3.5

Table 3.3 Properties of Fine aggregate

Sr. no	Characterstics	Value
1	Specific Gravity	2.46
2	Fineness modulus	2.56
3	Water absorption(%)	0.85

3.2.5 Water

Generally, water that is suitable for drinking is satisfactory for use in concrete. Water from lakes and streams that contain marine life also usually is suitable. When water is obtained from sources mentioned above, no sampling is necessary.

3.2.6 Reinforcing Steel

HYSD steel of grade Fe-500 Tata Tiscon steel of 12mm and 8mm diameters are used as longitudinal steel. 12mm dia bars are used as tension reinforcement and 8mm bars are used as compression steel and steel of 8mm diameter bars are used as shear stirrups.

3.2.7 Concrete Mix

Concrete mix is prepared using 53 grade Portland pozzolana cement, fine aggregate (medium-sized natural river sand) and crushed stone coarse aggregate with nominal size of 20 mm. The mix is taken as a nominal mix of M20 and as per Indian Standard Guidelines, the ratio of cement: sand: aggregate taken is 1:1.5:3. The water-cement ratio is 0.5 and compressive strength of concrete after 28 days is 29 MPa.

3.2.8 CFRP Material

Unidirectional CFRP sheets 300 mm wide and 0.117mm thickness are used for the retrofitting. The CFRP sheets are obtained from BASF construction chemicals and building systems shown in Fig 3.1. Under stress, fibre utilizes the plastic flow of matrix to transfer the load to the fibre which results in high strength and high modulus composite. Properties of the fibre used are given in Table 3.4. Main function of matrix is to combine and to protect the fibre against external environment into which the composite will be placed.

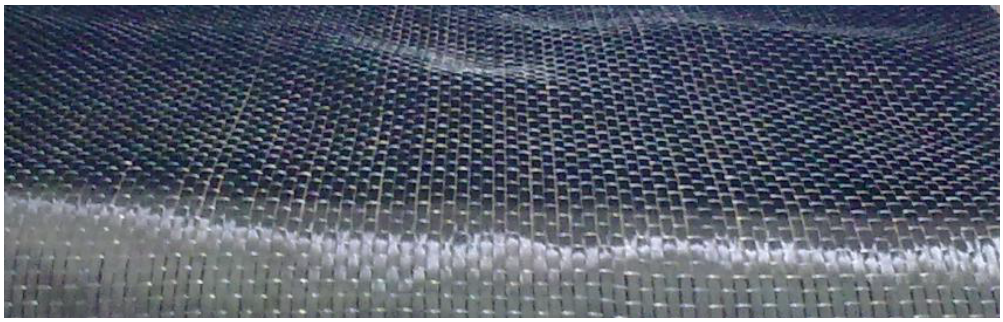

Fig. 3.1 Carbon Fiber sheet provided by BASF Ltd

Table 3.4 Technical Details of Fibres Provided by BASF Ltd

Sr.no	Technical data of fiber	230 gsm
1	Modulus of elasticity	230 kN/mm²
2	Tensile strength	4900 N/mm²
3	Weight of C fiber	200 g/m²
4	(main direction)	0.112 mm
5	Density	1.8 g/cm³
6	Ultimate strain%	1.50%

3.2.9 LVDT

The linear variable differential transformer (LVDT) is a type of electrical transformer used for measuring linear displacement. The transformer has three solenoid coils placed end-to-end around a tube. The centre coil is the primary, and the two outer coils are the secondary. A cylindrical ferromagnetic core, attached to the object whose position is to be measured, slides along the axis of the tube. The transducer which is used to calculate the deflections is of the range of 50mm and has the least count of 0.01mm shown in Fig 3.2. It is connected to the adapter box through wire and touched to the positions where the deflection is to be found out

Fig 3.2 Digital LVDT Used in Test

3.2.10 Adhesives

3.2.10.1 Primer

The adhesives used in the experiment were primer and epoxy. MasterBrace P 3500 is a two component solvent-less epoxy system which when mixed yields a penetrating medium viscosity primer. The primer was used for preparing a smooth surface for the application of the epoxy.

Fig. 3.3 Primer and its Hardner

Table 3.5 Technical Details of Primer Provided by BASF Ltd

Sr. no	Aspect Free	Flowing liquid
1	Mixed Density	1.07 ± 0.02 Kg/L
2	Volume solids	100%
3	Mixing ratio, by weight	100(Base):50 Hardner
4	Coverage	4-6 m^2 per Kg
5	Pot Life	40 Minutes at 25°C
6	Tack Free Time	6 Hours at 25°C
		3 Hours at 40°C
7	Adhesive bond strength to	> 1 MPa or concrete
	concrete (ASTM D4541	failure

3.2.10.2 Epoxy

MasterBrace 4500 is used to saturate the **MasterBrace** carbon, sheets to create a composite with the structure It increase flexural, shear, and axial load capacity The adhesive used for bonding FRP sheets with concrete is a compatible epoxy system provided by the manufacturer. It is blue pigmented epoxy resin for saturation of MBrace fibre sheet to form in-situ FRP Composite. It is made by mixing base saturant and hardner in ratio 100:40. Mixing of saturant and hardner is done thoroughly for five minutes until components are thoroughly dispersed. The properties of the adhesive saturant are shown in Table 3.6

Fig. 3.4 Epoxy and its Hardner

Table 3.6 Technical Details of Epoxy Provided by BASF Ltd

Sr no	Supply form	Translucent blue
1	Volume solids	100%
2	Mixed density (kg/l)	1.13 ± 0.03
3	Mixing ratio, by weight (A:B	100::40
4	Mixed viscosity (cps at	4000 ± 500
	25^{o}C)	
5	Pot life (minutes	25 min at 25^{o}C
6	Setting time	< 3hrs at 25^{o}C
		< 4hrs at 40^{o}C
7	Full cure	Full cure 7 days
8	Compressive strength	> 40 MPa at 1 day
	(ASTM C579)	> 60 MPa at 7 days
9	Flexural Strength	> 17 MPa
	(BS: 6319 Pt 3)	
10	Tensile Strength	> 35 MPa
	(BS: 6319 Pt 7)	

3.2.11 Roller

A special type of roller for impregnating the adhesive substance to the fibre and to the beam is used. The roller was provided by the manufacturer

3.2.12 Pre-stressing Machine

It is used to pre-stress the fibre sheet. Hydraulic jack is fitted in the machine with which force is applied and pre-stressing of fibre is done. On both the sides of this machine dial gauges are fixed to measure the elongation in fibre after applying the force. Front part of the machine iss curved and moveable as shown in Fig 3.5.

Fig 3.5 Prestressing Machine in Right and Hydraulic Jack in Left to Move the Rotating Arm

3.2.13 Anchor Bolts

12 mm diameter Anchor bolts are used to fasten the plates of pre-stressing machines. This bolt consists of two parts, bolt and rod. The rod when pushed inside bolt opens the bottom most part and creates a rigid hold.

3.2.14 Hydraulic Jack

Hydraulic jack was used to apply the load. Range of Hydraulic jack is 200 kN. (fig. 3.5)

3.3 DETAILING OF BEAM

The beam was designed to behave as under-reinforced section with M20 grade concrete and Fe500 steel of cross dimensions 13`6``×2`×1` (4100×600×300 mm). The reinforcement to be provided is 4 bars of 8 mm diameter in the compression zone and 4 bars of 12 mm diameter in the tension zone. Stirrups are also provided as 4-legged stirrups with 75mm spacing centre to centre. The detailed structural detailing of the beam is shown in Fig 3.6.

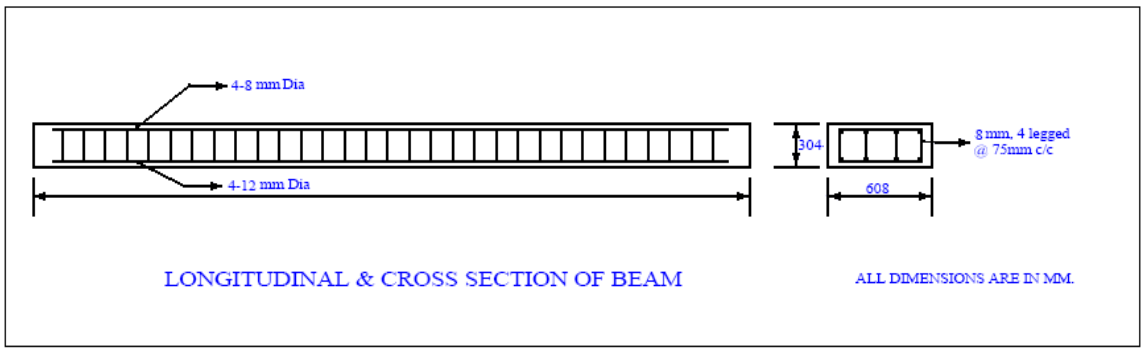

Fig 3.6 Details of Beam Used for Testing

3.4 TESTING ARRANGEMENT

To implement the desired objectives, twelve samples were tested. Samples were pasted on damaged and undamaged beam

Table 3.6 Details of Specimen for Present Research

SAMPLE	TYPE OF SURFACE
S1	UNDAMAGED
S2	
S3	GROOVED
S4	
S5	
S6	HOLED
S7	
S8	
S9	DAMAGED
S10	
S11	

In controlled sample the beam was undamaged and two samples were tested on it. Three grooves of 7 mm wide and 10 mm (approximately) were cut on the beam. The grooves were spaced from each other and edge approximately at a distance of 62.5 mm. The excess dust was removed and proper priming was done. In the holed sample three holes were drilled with the help of hammer drill on beam surface. The depth was

limited to 10 mm. The main idea was to penetrate the epoxy within the concrete. All these samples have pasted dimension of 250 X 75 mm.

Beam was grinded with the help of grinder having Diamond Plates. Purpose of grinding was to expose the aggregates so as to have better adhesion of the aggregates with the fibre.

Fig 3.7 Grinding of the Beam with Hand Grinder and Exposed Aggregates after Grinding

The pre-stressing machine setup consists of an arrangement which is to be fixed properly to the soffit of the beam. It consists of three parts:

1. Machine fixed to the beam.
2. Movable arm connected to the machine.
3. Plate which is to be anchored on the beam on the other side of the beam where machine is fixed.

For this, holes were drilled in the beam and fasteners of 12mm size were anchored inside by hammering its rod shown in Fig. 3.8 in on both the sides of the beam. The machine and the plate are anchored to it which is tightened through nuts.

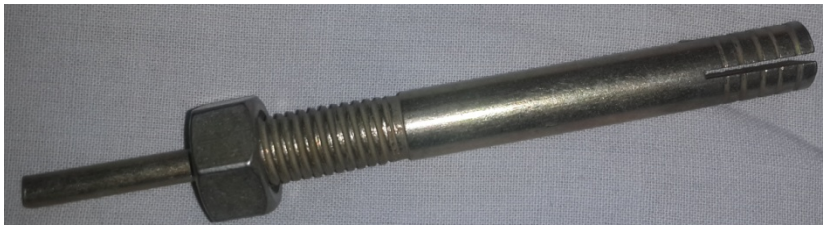

Fig 3.8 12 mm Anchored Bolts Used for Fastening Prestressed Machine

The machine was shifted six times on the controlled beam and accordingly the position of drills were marked and drilled. The beam was primed with master brace

3500 part A and Part B. Before application all grease, oil, dust residual curing compound, mould release agent or other contaminants that could impair adhesion were removed. Component A was mechanically mixed before adding component B. When component B has been added, mix for approximately 2 minutes or until a homogenous mix has been obtained. MasterBrace P 3500 as primer using roller or brush and wait until dry for the adhesive application. An overnight curing period was sufficient for the primer to get dry.

Fig. 3.9 Beam Primed with Master Brace 3500 Primer

Pasting Of sheet with Epoxy was done after the primed surface is once cleaned with the brush. Part A was thoroughly stirred and after adding Part B it was thoroughly blended. The ratio of Part A to Part B was kept 2.5:1. The mix once made has to be used in less than 30 minutes therefore FRP sheets cutting in proper size should be done prior to mixing.

Pre-stressing machine is anchored on one side of the beam over the sheets. The sheets are taken to the front movable portion of the machine, pasted to it through epoxy made in the proportion 100 (Base): 40 (Hardener). The movable part of the machine is further fixed by another plate below the FRP sheets, which are fastened together with bolts to make proper grip of sheet so that uniform force should be applied

Fig 3.10 Pasting of Sheet and Fixing of Prestressing Machine

LVDTS were used to find out the slip in FRP. For this a new system was prepared by using aluminium angle. The angle was fixed on FRP sheet with the help of same epoxy used to paste sheets. The angle doesn't have any contact with concrete surface and will move only when FRP sheet displaces. Therefore it prove to be good benchmark to measure slip.

Fig 3.11 LVDT's for the Measurement of Slips in FRP With Reference To Aluminium Angle

Another LVDT was used to measure the movement of movable arm which eventually tells us the elongation in the carbon fibre. The readings were taken at different elongation values and corresponding load was calculated by simple mechanics relation of stress and strain. The value of Elastic modulus for FRP was provided by the manufacturer.

Fig 3.12 LVDT Placed to Measure The Elongation in FRP Sheet

CHAPTER-4 RESULTS AND DISCUSSIONS

4.1 INTRODUCTION

In the present work the bond of FRP is studied with the concrete substrate. In different flexural tests the FRP fails in debonding. The idea behind this study was to relate the shear stresses produced in the direct pull off test with that of shear stresses generated in flexural testing. To achieve these eleven samples were tested. There were four categories and three sample fall in three categories and two samples in control test category. The tests were performed while producing different surface condition. These results were than compared with different models to study the strain distribution and bond slip relationships. Furthermore, results were compared with the previous study by Sharma. R (2013)

4.2 EXPERIMENTAL RESULTS

The experimental results for different samples are presented in this section. The samples are categorized as follows.

1. Controlled Sample. The samples were tested on undamaged beam and are designated by S1 and S2.

2. Grooved samples. The samples were pasted on beam with grooves and were tested. These are designated by S3, S4 and S5

3. Holed samples. The holes were drilled on beam and were filled with appropriate epoxy. The samples in this category are designated by S6, S7 and S8

4. Samples on damaged beam. The beam was taken which failed flexural loading. The samples in this category are designated by S9, S10 and S11

4.2.1Result of Controlled Sample (S1)

The controlled samples were tested on undamaged beam and were designated by S1 and S2. Given below are the results presented of controlled sample. From the results we can see that tensile cracks were visible at the shear stress of 4.66 N/mm^2 and finally the sheet was debonded at 5.76 N/mm^2 for S1. In fig 4.1 the tensile cracks are clearly visible. Ultimately at load of 108 kN the bond of fibre with the concrete failed by FRP rupture and delamination.

Table 4.1 Results of Sample S1

Slip		Slip avg.	Corresponding Load	Shear stress	Failure remarks
LVDT1	LVDT2	Mm	In kN.	N/mm2	
0	0	0	10.05	0.54	
0.01	0	0.005	18.29	0.98	
0.02	0.01	0.015	33.91	1.81	
0.02	0.01	0.015	44.91	2.40	
0.03	0.01	0.02	74.88	3.99	Debonding started
0.03	0.02	0.025	87.33	4.66	Cracks visible
0.03	0.02	0.025	107.93	5.76	Bond failed

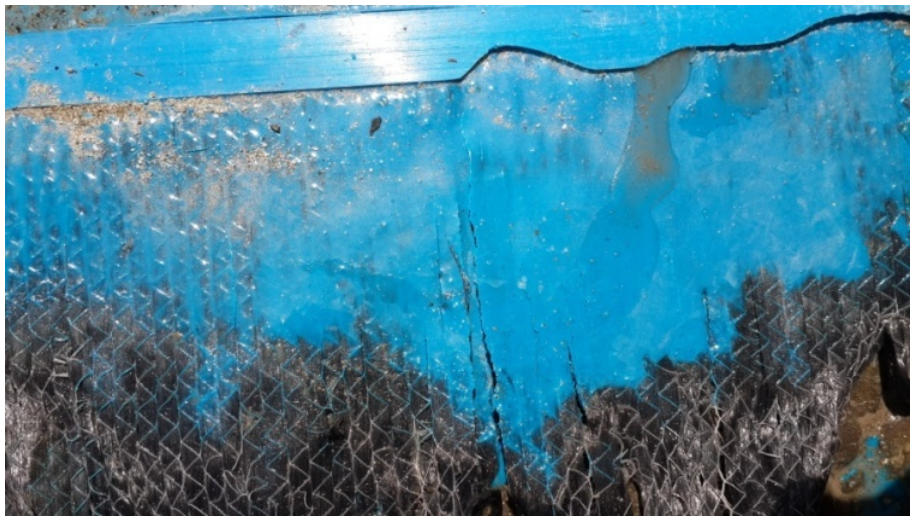

Fig. 4.1Tensile Cracks in S1 Sample

4.2.2 Result of controlled Sample (S2)

Table 4.2 Result of Sample S2

Slip(mm)		Slip avg.	Corresponding Load	Shear stress	Failure remarks
LVDT 1	LVDT 2	(mm)	In kN.	N/mm^2	
0	0	0	24.64	1.3143	
0.01	0.01	0.01	26.19	1.3968	
0.01	0.01	0.01	36.92	1.9692	
0.02	0.01	0.015	45.68	2.4363	
0.02	0.02	0.02	47.74	2.5462	
0.02	0.02	0.02	57.7	3.0775	Debonding started

0.03	0.02	0.025	65.43	3.4896	Cracks visible
0.03	0.03	0.03	105.96	5.6512	
0.03	0.03	0.03	114.37	6.1	Bond failed

From the above data we can see for the controlled sample S2 debonding of sheet was started at 45.68 kN. At this load the cracks were visible and failure of bond occurred at 114.37 kN.

The results for the controlled sample S1 and S2 showed that the shear stress value at failure were 5.76 N/mm^2 and 6.1 N/mm^2 with max avg. slip of 0.025 and 0.3 respectively. These stresses were generated at ultimate load at which the bond failed. However the debonding stage was appeared earlier in both the samples.

4.2.3 Result of Grooved Sample (S3)

Table 4.3 Results of S3

Slip(mm)		Slip avg.	Corresponding Load	Shear Stress	Failure Remarks
LVDT 1	LVDT 2	(mm)	In kN.	N/mm^2	
0	0.01	0.005	28.68	1.53	
0	0.01	0.005	38.3	2.04	
0	0.01	0.005	77.8	4.1	
0.01	0.01	0.01	92.22	4.9	
0.01	0.01	0.01	99.43	5.3	
0.01	0.02	0.015	110.42	5.9	Debonding started
0.02	0.02	0.02	118.67	6.3	
0.02	0.03	0.025	125.02	6.7	
0.02	0.03	0.025	130.86	7	
0.02	0.03	0.025	139.62	7.4	Bond Failure

The result from the above data shows that the groves sample has proved to show higher ultimate load than the control samples. The reason for this is increase in the surface contact area for concrete and epoxy. The debonding started at 110.42 kN, however no tensile cracks were visible and finally the bond failed at 139.62 kN . This was the failure of epoxy concrete bond (Fig 4.2).

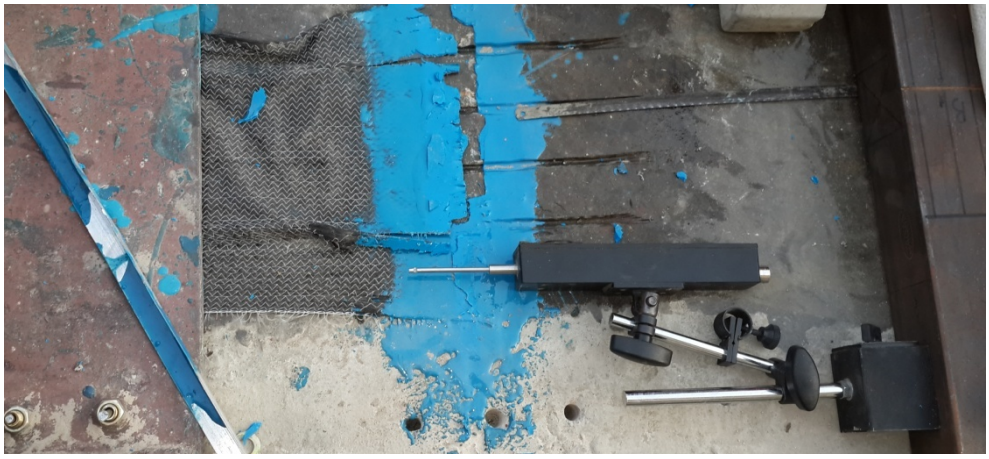

Fig 4.2 Bond Failure of the Grooved Sample

4.2.4 Results of Grooved Sample S4

Table 4.4 Results of Sample S4

Slip(mm)		Slip Avg.	P	Shear Stress	
LVDT1	LVDT2	(mm)	In kN	N/mm^2	Failure remarks
0	0	0	20.95	1.12	
0	0	0	24.73	1.32	
0	0	0	27.65	1.47	
0	0.01	0.005	30.4	1.62	
0	0.01	0.005	31.77	1.69	
0.01	0.01	0.01	33.14	1.77	
0.01	0.02	0.015	36.92	1.97	
0.01	0.02	0.015	37.95	2.02	
0.01	0.02	0.015	39.5	2.11	
0.01	0.02	0.015	41.39	2.21	
0.01	0.03	0.02	41.9	2.23	
0.02	0.03	0.025	44.65	2.38	
0.02	0.03	0.025	46.2	2.46	
0.02	0.03	0.025	49.63	2.65	
0.02	0.04	0.03	53.07	2.83	
0.03	0.05	0.04	55.64	2.97	
0.07	0.12	0.095	63.37	3.38	
0.07	0.14	0.105	78.83	4.2	
0.07	0.14	0.105	94.45	5.04	Debonding started
0.07	0.14	0.105	115.92	6.18	
0.07	0.15	0.11	128.46	6.85	
0.07	0.18	0.125	144.6	7.71	Bond Failure

The second sample of grooved category showed similar results as the first one. The ultimate load again was quite high as compare to control samples. The crackling sound at 94.45 kN could be heard and finally the sheet was peeled off at load 144.60 kN which is the ultimate load.

4.2.5 Results of Grooved Sample (S5)

Table 4.5 Results of sample S5

Slip (mm)		Slip avg.	P	Shear Stress	Failure
LVDT1	LVDT2	(mm)	In kN.	N/mm^2	Remarks
0	0	0	25.07	1.337	
0.01	0	0.005	28.85	1.539	
0.01	0.01	0.01	34	1.814	
0.01	0.01	0.01	38.64	2.061	
0.01	0.01	0.01	40.19	2.143	
0.2	0.01	0.105	44.14	2.354	
0.2	0.01	0.105	47.91	2.555	
0.2	0.2	0.2	48.94	2.61	
0.3	0.2	0.25	60.45	3.224	
0.3	0.02	0.16	78.31	4.177	
0.3	0.02	0.16	89.82	4.79	
0.04	0.02	0.03	114.55	6.109	Debonding started
0.04	0.02	0.03	123.48	6.585	
0.04	0.02	0.03	134.81	7.19	Bond Failure

Similarly the third sample of grooved type failed at load of 134.81 kN. In all the samples of grooved family the failing load was quite high as compare to samples on controlled beam.

4.2.6 Results of Holed Sample S6

Table 4.6 Results of Sample S6

Slip(mm)		Slip avg	P	Shear stress	Failure
LVDT1	LVDT2	(mm)	In kN	N/mm^2	remarks
0	0	0	10.65	0.5679	
0.01	0	0.005	21.12	1.1266	
0.01	0	0.005	26.96	1.438	

0.01	0.01	0.01	33.49	1.786	
0.02	0.01	0.015	41.22	2.1982	
0.02	0.01	0.015	49.63	2.647	
0.02	0.01	0.015	54.27	2.8943	
0.02	0.01	0.015	61.48	3.279	
0.03	0.01	0.02	78.31	4.1766	
0.03	0.01	0.02	83.98	4.4788	
0.03	0.02	0.025	87.76	4.6803	
0.03	0.02	0.025	90.33	4.8177	Bond Failure

In the holed sample S6 the ultimate load at failure was 90.33 kN and shear stress was 4.8 N/mm^2 at the failure. The failure mode here was sudden and brittle failure at comparative low load than the grooved category.

Fig.4.3 Failure of Sample S6

4.2.7 Results of Holed sample S7

Table 4.7 Results of Sample S7

Slip(mm)		Slip Avg	P	Shear Stress	Failure
LVDT1	LVDT2	(mm)	In kN	N/mm^2	Remarks
0	0	0	3.95	0.211	
0	0	0	9.79	0.522	
0.01	0	0.005	14.25	0.76	
0.01	0.01	0.01	19.75	1.053	
0.01	0.01	0.01	33.66	1.795	
0.01	0.02	0.015	36.92	1.969	
0.01	0.02	0.015	47.23	2.519	
0.01	0.02	0.015	50.32	2.684	
0.01	0.02	0.015	53.58	2.858	

0.02	0.02	0.02	63.2	3.371	
0.02	0.02	0.02	67.83	3.618	
0.02	0.02	0.02	70.93	3.783	
0.02	0.02	0.02	78.31	4.177	
0.02	0.02	0.02	89.82	4.79	
0.02	0.02	0.02	97.03	5.175	
0.03	0.02	0.025	100.81	5.376	Debonding started
0.03	0.02	0.025	105.62	5.633	
0.03	0.02	0.025	113.86	6.072	
0.03	0.02	0.025	119.53	6.375	
0.03	0.02	0.025	124.51	6.64	Bond failure

The result obtained from the sample S7 testing showed a failure load of 124.51 kN. and the stress at failure was 6.64 N/mm^2. Sudden debonding failure was observed in comparatively lower loads than grooved samples.

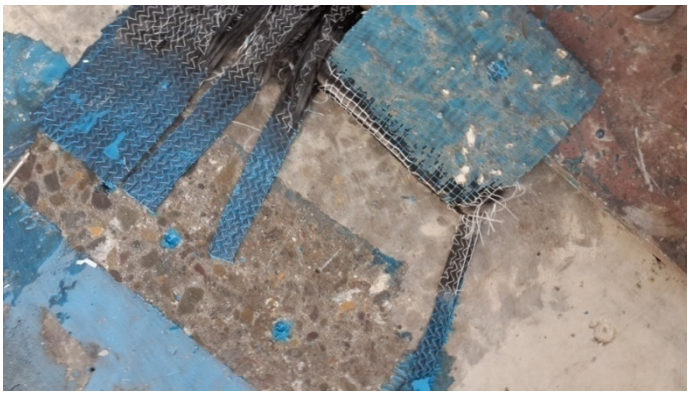

Fig.4.4 Sample S7 after Debonding

4.2.8 Results of Holed Sample S8

Table 4.8 Results of Sample S8

Slip(mm)		Slip Avg	Corresponding Load	Shear Stress	Failure
LVDT1	LVDT2	(mm)	In kN	N/mm^2	Remarks
0	0	0	0.55	0.029	
0.01	0	0.005	1.44	0.077	
0.01	0	0.005	1.65	0.088	
0.01	0.01	0.01	19.75	1.053	
0.02	0.01	0.015	29.02	1.548	
0.02	0.01	0.015	33.66	1.795	

0.02	0.01	0.015	38.98	2.079	
0.02	0.01	0.015	44.82	2.391	
0.03	0.01	0.02	58.9	3.142	
0.03	0.01	0.02	66.8	3.563	
0.03	0.02	0.025	75.91	4.048	
0.03	0.02	0.025	82.09	4.378	
0.03	0.02	0.025	88.1	4.699	
0.03	0.02	0.025	97.03	5.175	
0.03	0.02	0.025	106.99	5.706	Bond failure

The ultimate load for sample S8 was 106.99 kN . If we compare the results with that of undamaged sample we realize there was not much effect of drilling the sample. The results were in the range of controlled samples.

4.2.9 Results of Sample on Damaged Beam (S9)

Table 4.9 Results of Sample S9

Slip(mm)		Avg Slip	P	Shear Stress	Failure
LVDT1	LVDT2	(mm)	In kN	N/mm^2	Remarks
0	0	0	15.28	0.8152	
0.01	0	0.005	45.17	2.4088	
0.01	0	0.005	54.44	2.9034	
0.01	0.01	0.01	66.12	3.5263	
0.01	0.01	0.01	76.42	4.0758	
0.01	0.02	0.015	82.78	4.4147	
0.01	0.02	0.015	88.44	4.7169	
0.01	0.03	0.02	101.67	5.4222	
0.01	0.03	0.02	107.16	5.7153	Bond Failure

The samples tested on damaged beam showed a different mode of failure. The shear failure of concrete was observed only in case of the damaged samples. However the ultimate load of failure for undamaged samples also is in same range as damaged but with different mode of failure.

4.2.10 Results of Sample on Damaged Beam (S10)

Table 4.10 Results of Sample S10

Slip(mm)		Slip avg.	P	Shear Stress	Failure
LVDT1	LVDT2	(mm)	In kN	N/mm^2	Remarks
0	0	0	43.28	2.37	
0.01	0.01	0.01	54.1	2.96	
0.02	0.01	0.015	66.12	3.62	
0.03	0.02	0.025	70.75	3.88	
0.03	0.02	0.025	76.08	4.17	
0.04	0.03	0.035	83.98	4.6	
0.04	0.03	0.035	89.3	4.89	
0.04	0.03	0.035	93.59	5.13	
0.05	0.03	0.04	99.61	5.46	
0.05	0.03	0.04	105.1	5.76	
0.05	0.03	0.04	110.77	6.07	
0.05	0.03	0.04	115.58	6.33	Bond failure

Fig. 4.5 Failure of Sample on Undamaged Beam S10

The ultimate load of failure for S10 was 115.58 kN and stress at failure was 6.33 N/mm^2. Here also shear failure of concrete was observed.

4.2.11 Result of Sample on Damaged Beam (S11)

Table 4.11 Results of Sample S11

Slip(mm)		Avg slip	Corresponding Load	Shear Stress	Failure
LVDT 1	LVDT 2	(mm)	In kN	N/mm^2	Remarks
0	0	0	26.96	1.44	
0	0	0	38.64	2.06	
0.01	0	0.005	58.9	3.14	
0.01	0	0.005	64.92	3.46	
0.01	0.01	0.01	70.75	3.77	
0.01	0.01	0.01	72.64	3.87	
0.01	0.01	0.01	78.31	4.18	
0.02	0.01	0.015	83.98	4.48	
0.03	0.02	0.025	87.93	4.69	Debonding started
0.03	0.02	0.025	97.03	5.17	
0.03	0.03	0.03	99.26	5.29	Visible Cracks
0.03	0.03	0.03	101.84	5.43	
0.04	0.03	0.035	107.51	5.73	
0.04	0.03	0.035	110.25	5.88	
0.04	0.03	0.035	117.81	6.28	
0.05	0.03	0.04	118.84	6.34	
0.05	0.03	0.04	124.33	6.63	Complete Debonding

In the damaged beam sample the loading ranges were almost fall in the range of controlled sample. But a interesting feature which came into picture was shear failure of concrete. Fig 4.5 & Fig 4.6 shows the delamination along with the shear failure of concrete. In no samples other than damaged beam samples this type of failure was seen. This explains the stresses at the failure was enough to fail the concrete in shear.

Fig.4.6 Sample S11 Failed due to Concrete Shear

4.3 ANALYSIS OF RESULTS

The results obtained were used to develop the strain distribution pattern along the length of sheet as well as bond slip model was analysed and experimental results were compared with it. The Two models were chosen to elaborate the study in a more precise way, namely

1.The analytical model was chosen and with the help of it strain distribution was Studied in elastic as well as inelastic zone by Ming Z. et al., (2004)

2. The analytical model chosen for the detailed discussion on bond slip analysis. The present thesis work was compared with the existing precise simplified model by Lu X Z et al., (2005)

4.3.1 Analysis of Ming and Ansari (2004) model

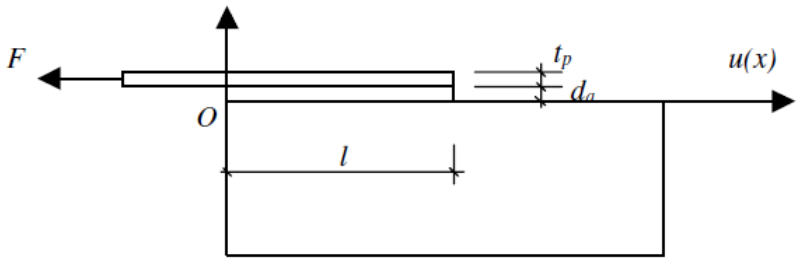

Fig 4.7 Computed Model for Elastic Analysis (Ming and Ansari., 2004)

The shear angle was defined in the longitudinal direction of the epoxy adhesive as follows

$$\gamma a = u_p / d_a \quad (1)$$

in which, *up* is the displacement of the FRP sheet, *da* is the thickness of the epoxy adhesive layer. According the relation between and shear stress along the longitudinal direction

$$\tau_a = G_a \gamma a = \frac{Ga}{da} u_p \quad (2)$$

where, *Ga* is the shear modulus of the adhesive

thus,

$$\frac{d\tau a}{dx} = \frac{Ga}{da} \frac{dup}{dx} = \frac{Ga}{da} \varepsilon_p = \frac{Ga}{Ep * da} * \sigma_p \quad (3)$$

in which, *Ep* is the elastic modulus of FRP sheet, and σ_p is the normal in plane stress along the longitudinal direction. And

$$\frac{d^2 \tau_a}{dx^2} = \frac{G_a}{E_p d_a} \frac{d\sigma_p}{dx} = \frac{G_a}{E_p d_a t_p} \tau_a \quad (4)$$

in which, *tp* is the thickness of the FRP sheet

$$\frac{d^2 \tau_a}{dx^2} - \alpha^2 \tau_a = 0 \quad (5)$$

in which

$$\alpha^2 = \frac{G_a}{E_p d_a t_p} \quad (6)$$

This is a 2nd order ordinary differential equation, and the solution can be expressed as follows:

$$\tau_a = B \cosh \alpha x + C \sinh \alpha x \quad (7)$$

The tests conducted by the author failed in concrete shear always. Thus, they have divided the whole loading process into two parts:

(1) initial part: at this stage, there is no damage in concrete and FRP fabrics and the adhesive materials; and

(2) non linear part. At this stage, the shear cracks have formed at the front part of the fabrics.

At the initial elastic stage, the boundary conditions of equation (1) are:

$$\varepsilon_p(x=l)=0$$

$$\varepsilon_p(x=0)=\frac{F}{E_pA_p}$$

where, *F* is the tension acting on the FRP sheet, *Ap* is the area of FRP sheet. From these bondary conditions, the coefficients of Eq. (6) can be solved:

$$B=-\frac{G_a l\tau_m}{\alpha d_a E_p t_p}\frac{1}{\tanh\alpha l},\ C=\frac{G_a l\tau_m}{\alpha d_a E_p t_p}\ \text{and}\ \tau_m=\frac{F}{b_p l}$$

Thus, the solution of Equation (5) is:

$$\tau=\frac{G_a l\tau_m}{\alpha d_a E_p t_p}(\sinh\alpha x-\frac{\cosh\alpha x}{\tanh\alpha l}) \tag{7}$$

From Eq.(3) we can get the strain distribution of the FRP fabrics:

$$\varepsilon_p=\frac{l\tau_m}{E_p t_p}(\cosh\alpha x-\frac{\sinh\alpha x}{\tanh\alpha l}) \tag{8}$$

The constants used are

E_p=	230000	N/mm²
$A_{p=}$	28	mm^2
Ga=	1460	N/mm^2
L=	75	mm
tp=	0.112	mm
da=	1	mm

At the 2nd nonlinear stage, failure will occure at the tension end zone due to high shear stress in the concrete layer beside the FRP sheet while the rest part remains elastic (Fig. 7).

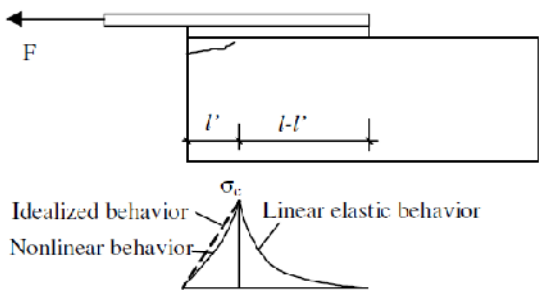

Fig 4.8 Computed Model for Nonlinear Analysis

shear stress can be express as

$$\tau = -\frac{x}{l'}\tau_c \text{ when } 0 \le x < l' \tag{9}$$

In the elastic region, the expression of τ is same as (7), only the coefficient has to be changed. The expression is writen as follows:

$$\tau = \tau_c \tanh[\alpha(l-l')](\sinh[\alpha(x-l')] - \frac{\cosh[\alpha(x-l')]}{\tanh[\alpha(l-l')]}) \text{ when } l' < x < l \tag{10}$$

The strain distribution can be written as:

$$\varepsilon_p = \frac{l}{E_p t_p}(\tau_m - \frac{x^2}{2ll'}\tau_c) \text{ when } 0 \le x < l' \tag{11}$$

$$\varepsilon_p = \frac{\alpha d_a \tanh[\alpha(l-l')]}{G_a}(\cosh[\alpha(x-l')] - \frac{\sinh[\alpha(x-l')]}{\tanh[\alpha(l-l')]})\tau_c \text{ when } l' \le x \le l \tag{12}$$

The above relations for elastic and inelastic zone were used to compute shear stresses and strain distributions along FRP's.

4.3.2 Analysis of Lu X. Z et al., (2005) model

This model was used to compare the bond slip test results with that of analytical precise model in simplified form. The precise model is accurate but complicated therefore a simplification of it was done without any loss of accuracy.

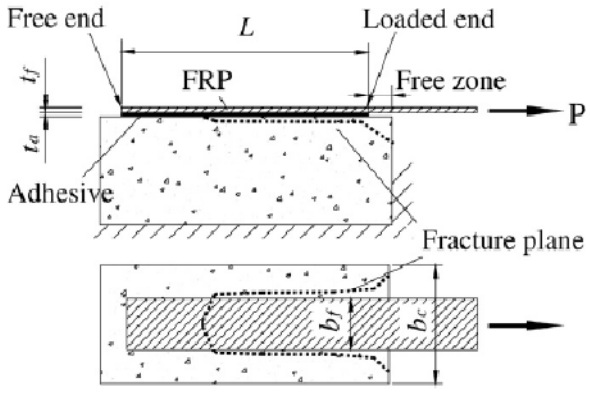

Fig 4.9 Generalized Schematic Bond Test X.Z. Lu et al., (2005)

The following equations were used to find out the analytical results.

$$\tau = \tau_{\max}\sqrt{\frac{s}{s_0}} \qquad \text{if } s \le s_0 \tag{13}$$

$$\tau = \tau_{\max} e^{-\alpha\left(\frac{s}{s_0}-1\right)} \qquad \text{if } s > s_0 \tag{14}$$

Where τ_{max} is the maximum shear and s_o is the corresponding slip. s is the slip which was kept variable and corresponding shear stresses were calculated. The value these variable were calculated as

$$\tau_{\max} = \alpha_1 \beta_w f_t \tag{15}$$

$$s_0 = 0.0195 \beta_w f_t \tag{16}$$

and $$G\,f = 0.308\beta^2{}_w f_t \tag{17}$$

From the above relations the values were calculated for specimen as $\beta w=1.05718828, S_O= 0.0777$, $G_{0=}0.6685, \alpha=1.295$ and $\tau max=5.977$ N/mm^2 . Putting these values in eq 13 and 14 we can find out value of shear stress bu keeping s variable. Hence from these finite element results, the following observations can be made:

(a) The bond–slip curve is made up of an ascending branch and a descending branch, with the bond stress reducing to zero when the slip is sufficiently large.

(b) The initial stiffness of the bond–slip curve is much larger than the secant stiffness at the peak stress point. This initial high stiffness, representing the stiffness of the completely linear elastic state of the interface, decreases quickly with the appearance of microcracking in the concrete as the bond stress increases.

(c) The maximum bond stress τmax and the corresponding slip s0 increase almost linearly with ft, while the interfacial fracture energy $G\,f$ increases almost linearly with $\sqrt{ft}$,

4.4 Comparison of Results

In this section the specimen results were computed according to the existing models explained above.

4.4.1Analysis of Controlled Sample S1

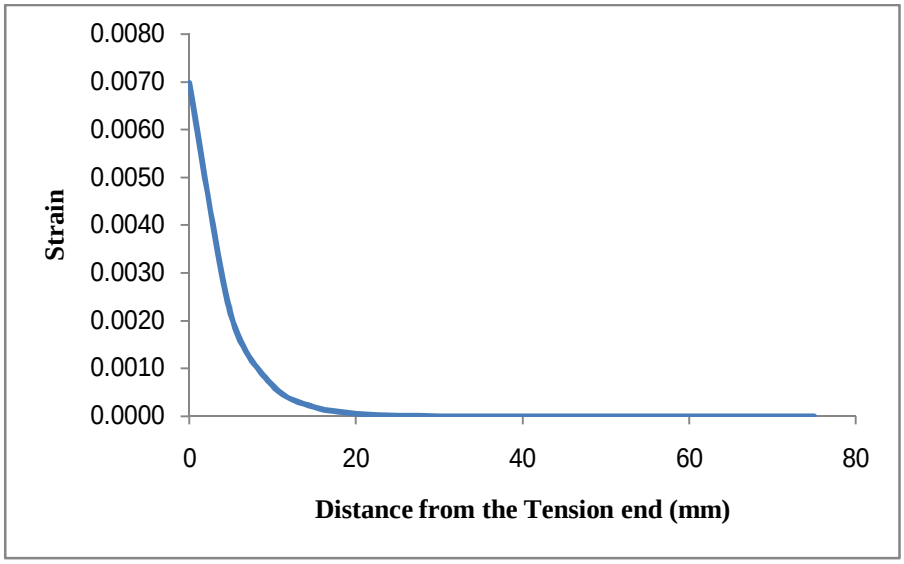

Fig 4.10 Strain Distribution for S1 Sample in Elastic Zone at Load of 44.91 kN

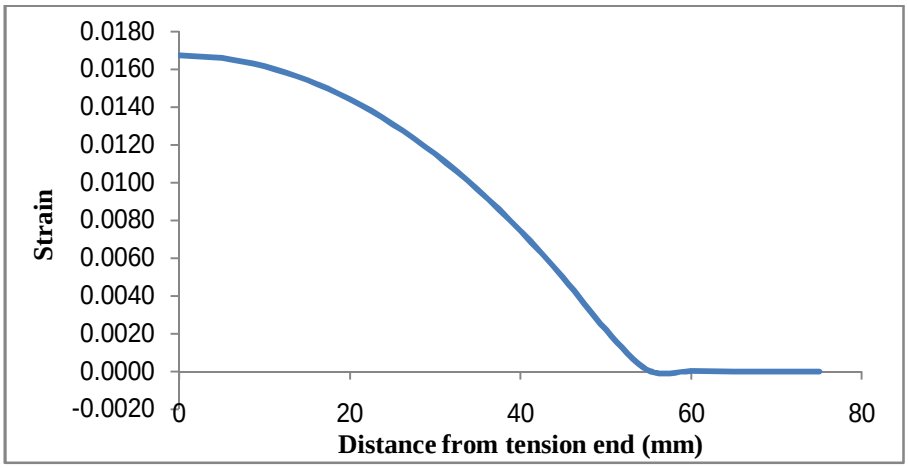

Fig. 4.11 Strain Distribution for S1 Sample in Inelastic Zone at Load Of 107.93 Kn

For studying the strain distribution the equation 7 to 12 were solved and graphs were prepared. These graphs were satisfactory with the results of the model proposed by Mind and Ansari (2004). In the elastic stage we can see that the strain beyond 20 mm length tends to be zero and in the inelastic stage just before the bond failure the strains were decreasing gradually with maximum at the tension end and min at a distance of about 57 mm from the tension end. From the bond slip analysis the value of S_o was around 0.0771 calculated from eq 16. And corresponding value of shear stress was

5.67 N/mm^2. Since the actual stress at which sample failed was 5.96 N/mm^2 (solving eq. 13) we found the maximum stress at failure was very close to that of experimental value. Hence the experimental result was satisfactory with the model.

4.4.2 Analysis of Controlled Sample S2

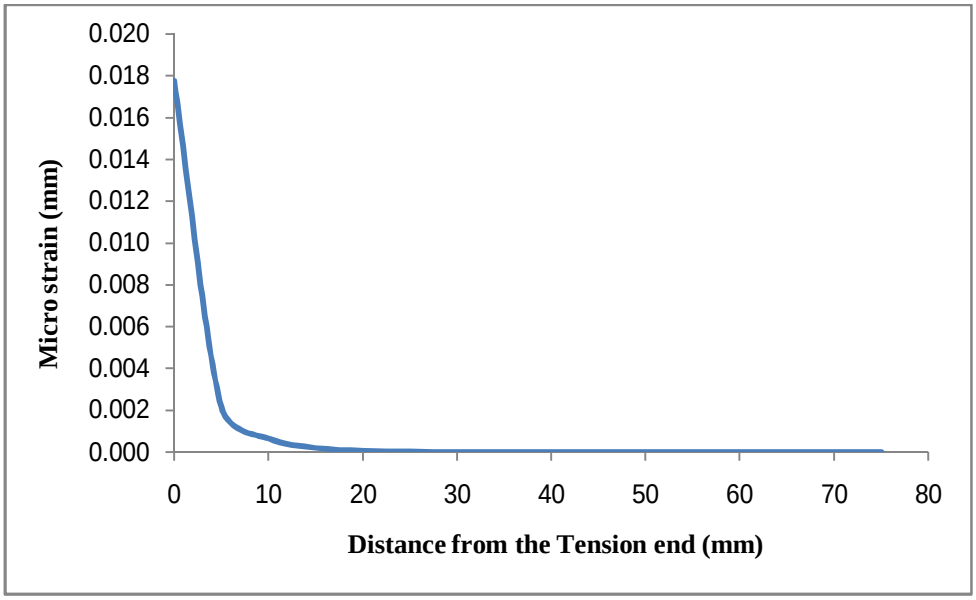

Fig 4.12 Strain Distribution for S2 Sample in Elastic Zone At Load of 45.68KN

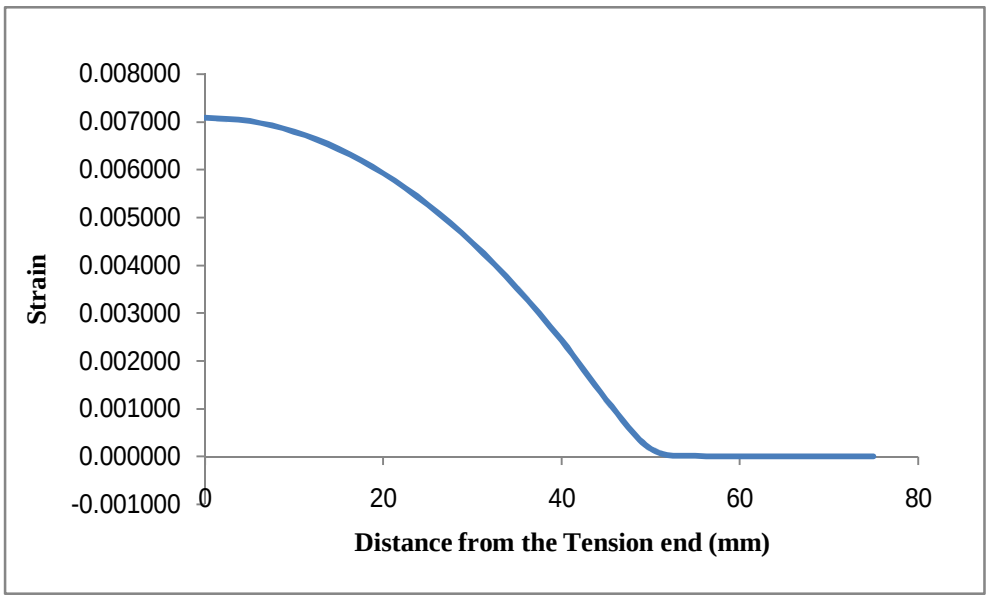

Fig. 4.13 Strain Distribution for S2 Sample in inelastic Zone at Load of 114.37 kN

The strain distribution for sample S2 was quite similar to the sample S1. Since it is interesting to note from equation eq. 8 that the value of the strain are dependent on the

hyperbolic value of x which varies in same pattern for the all samples but however the major difference can only be seen when there is difference in the value of τm which is the shear stress at the debonding. This value is actually almost same in both cases as a result we got same results in strain distribution. The shear stress at which sample failed was 6.1 N/mm^2 and solving eq. 13 the value of shear was 5.96 N/mm^2. Hence we found these two values are very close therefore the result for this sample was satisfactory with that of Lu X.Z et al., (2005) model.

4.4.3 Analysis of Grooved Sample S3

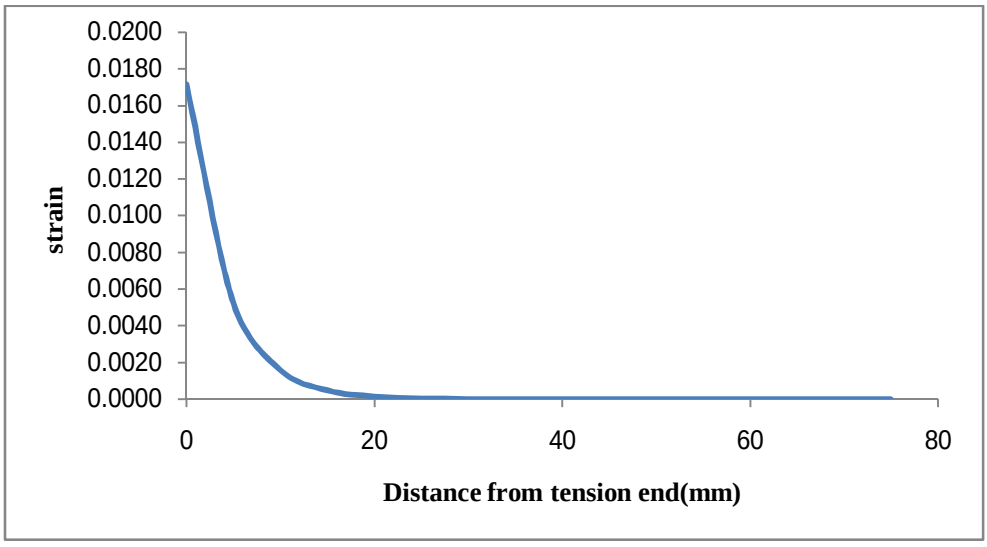

Fig 4.14 Strain Distribution for S3 Sample In Elastic Zone At Load Of 110.42KN

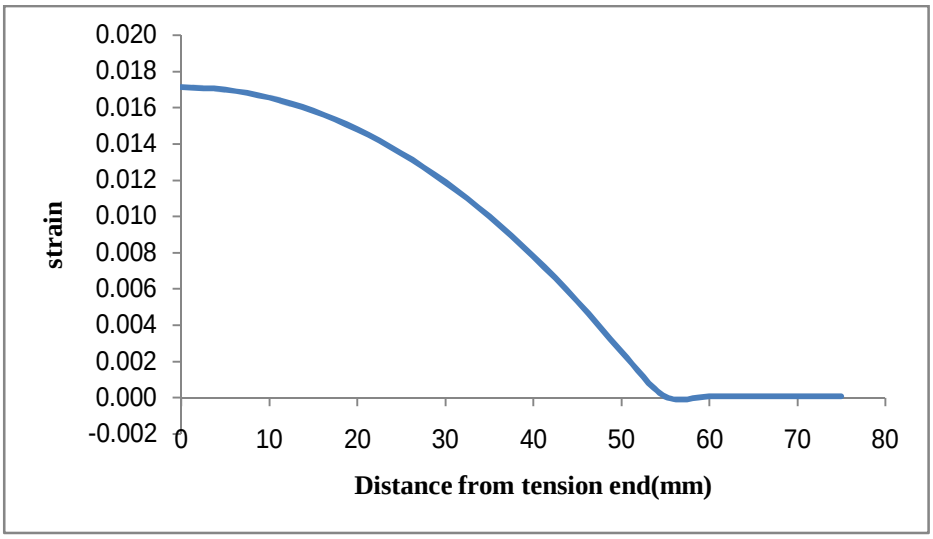

Fig 4.15 Strain Distribution for S3 Sample in Inelastic Zone At Load Of 139.62 kN

The grooved surface with appropriate filling of epoxy showed good results as compare to any other surface preparation. Due to increase in surface contact area the samples were capable of undertaking higher loads. The strain distribution profile in inelastic zone indicates the strain getting zero after 55 mm. Therefore the bond length for this specimen can be taken as 55 mm. The max stress in experimental result was 7.4 N/mm^2 and the analytical value is 5.96 N/mm^2, hence the experimental results were not confined to that of analytical model. One reason for such high shear stresses in grooved sample is the increase in contact area of epoxy resin with the concrete surface.

4.4.4 Analysis of Grooved Sample S4

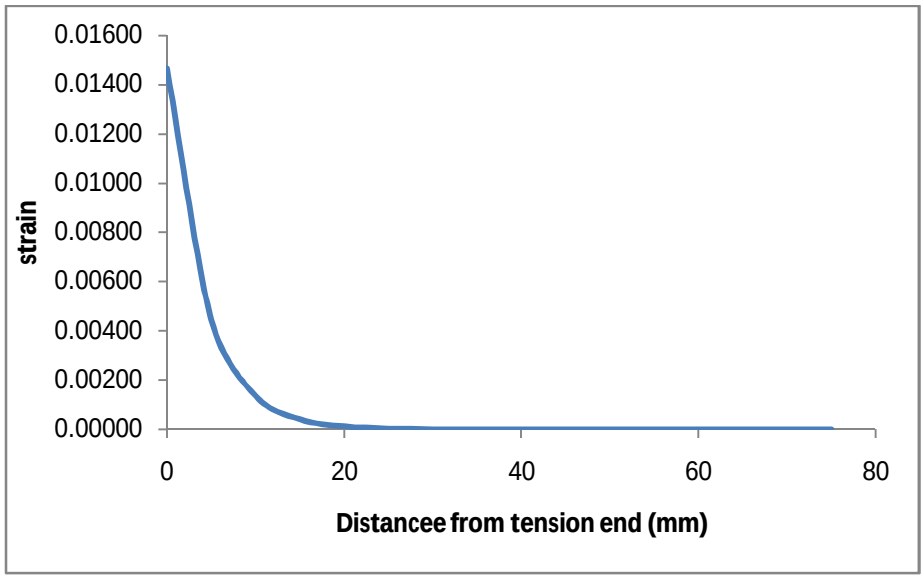

Fig 4.16 Strain Distribution For S4 Sample In Elastic Zone at Load of 94.45KN

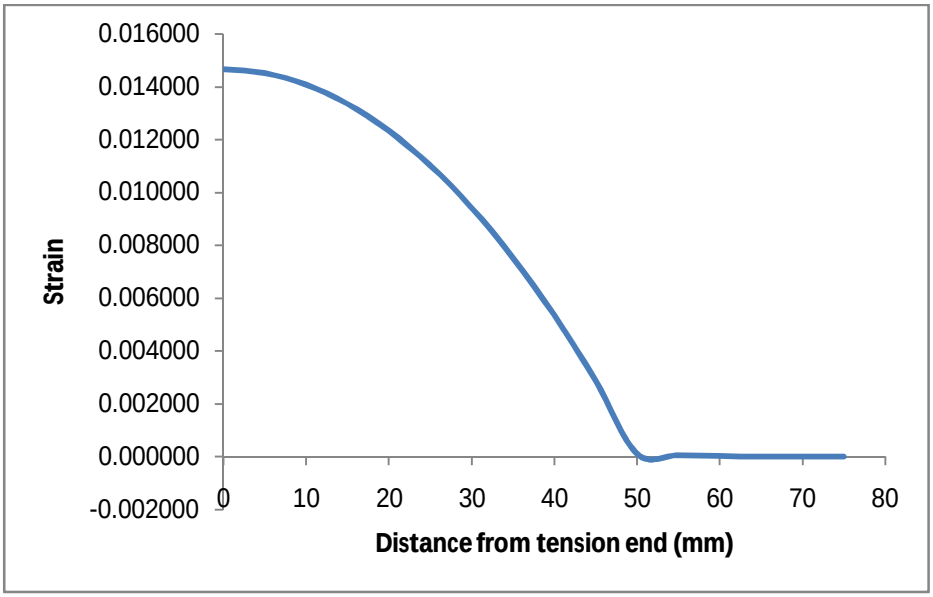

Fig 4.17 Strain Distribution for S4 Sample in Inelastic Zone at Load Of 144.60 kN

The Sample S4 showed the similar results as S3. The strain distribution in inelastic stage tends to zero beyond 50 mm. Therefore the bond length of the specimen can be taken as 50 mm. In the bond slip model the experimental results are obtained within the range of analytical results. The maximum stress in analytical curve is 5.96 N/mm^2 and that of experimental is 7.71 N/mm^2 and thus has great difference.

4.4.5 Analysis of Grooved Sample S5

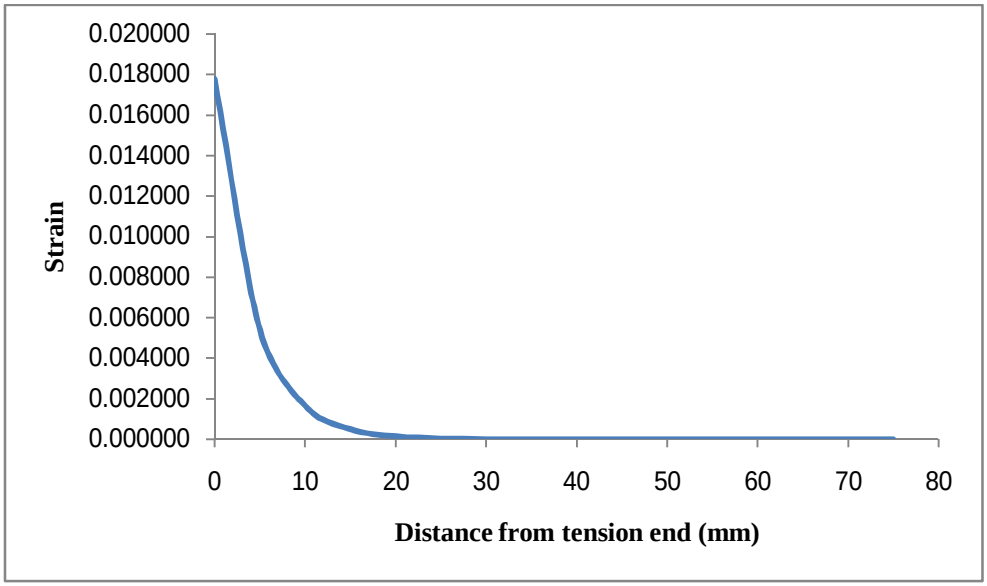

Figure4.18 Strain Distribution For S5 Sample in Elastic Zone at Load Of 114.55KN

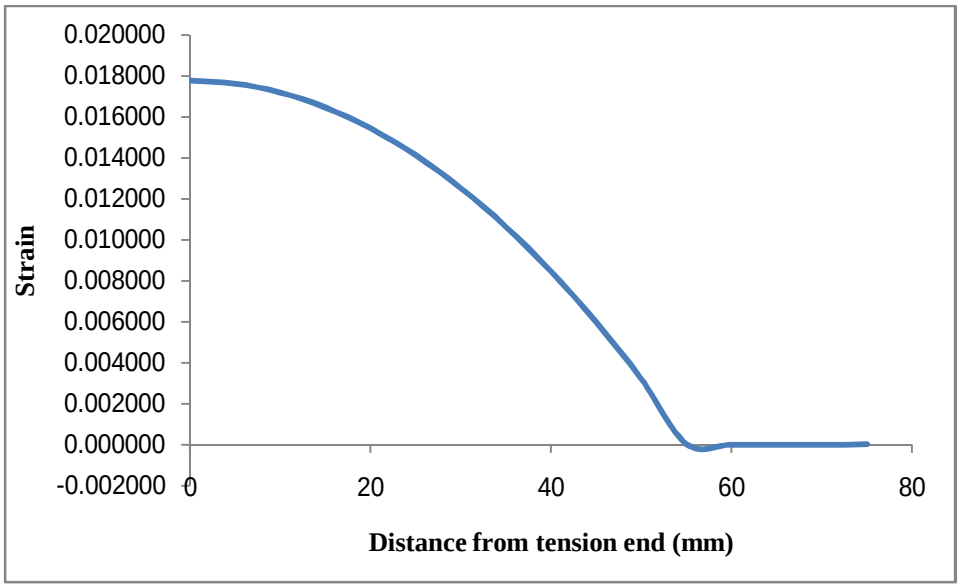

Fig 4.19 Strain distribution for S5 Sample in Inelastic zone at Load of 134.81 kN

In inelastic zone the curve tends to zero beyond 58 mm from the tension end. Thus the bond lentgth for this specimen was taken as 58 mm. The shear stress from experimental result was 7.19N/mm^2 which is very high as compare to the analytical value of 5.96 N/mm^2. In the bond slip comparison the results of S3,S4,S5 were found to be similar. This is because of the increased surface area. The shear stresses are actually not evenly distributed beneath the sheet rather they are the function of hyperbolic function of distance from the tension end (eq. 7 and eq. 10). These equation does not account for any factor which talk about the modification due to enhanced increase in area because of grooving. The samples S3, S4 and S5 have however confirmed the delayed debonding process.

4.4.6 Analysis of Holed Sample S6

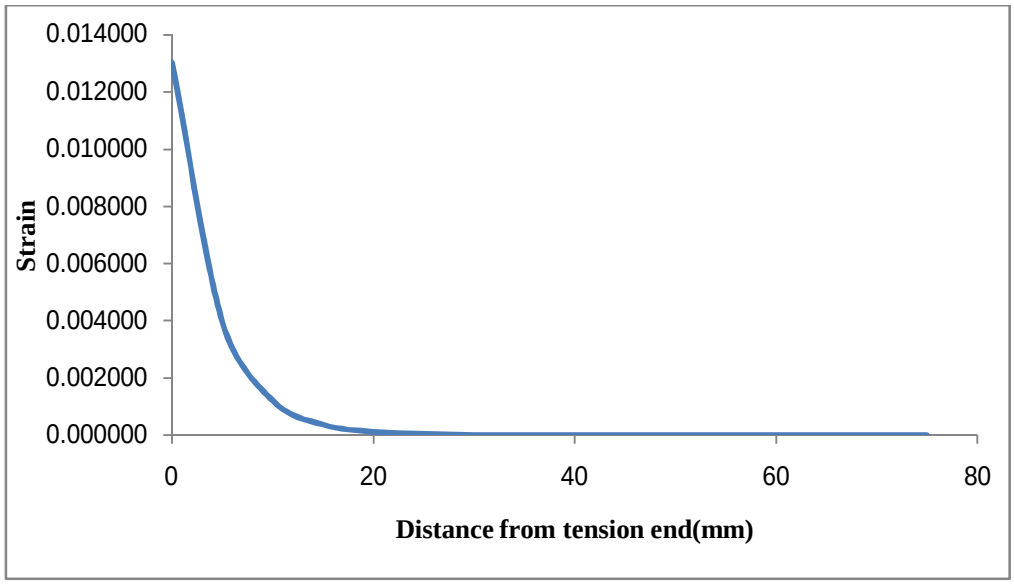

Fig 4.20 Strain distribution for S6 sample in Elastic Zone at Load of 83.98 kN

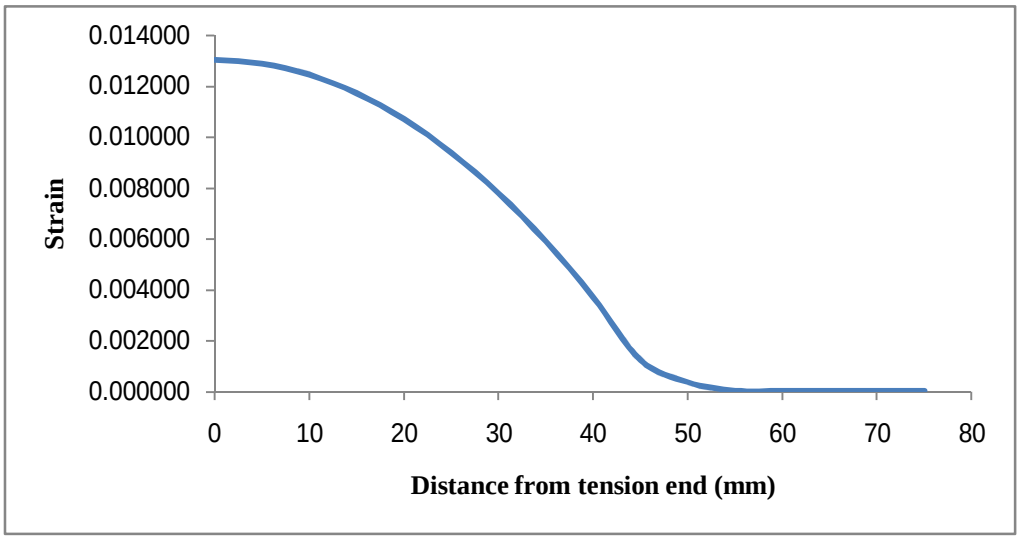

Fig 4.21Strain distribution for S6 Sample in Inelastic Zone at Load of 90.33 kN

Sample S6, S7 and S8 are the holed samples. In inelastic zone the curve tends to zero at 52 mm and hence bond length of this specimen can be taken as 52 mm. However our motive of achieving higher strength was not achieved because of the failure of bond between epoxy and concrete occurred prior to ultimate shear stresses of concrete. The Shear stress in experimental result was 4.8 N/mm^2 and less as compare to the analytical value of 5.96 N/mm^2.

4.4.7 Analysis Holed of Sample S7

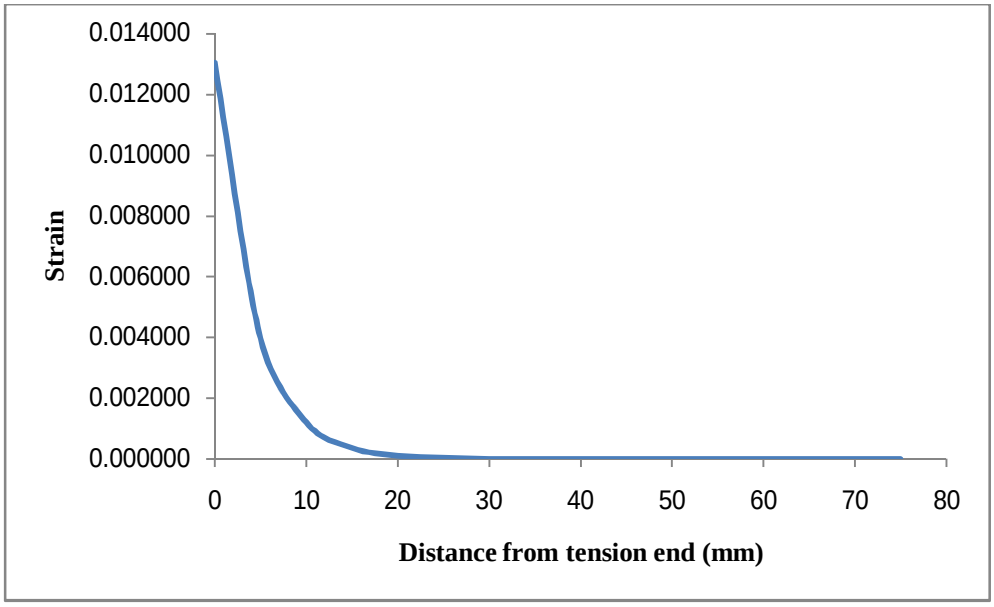

Fig. 4.22 Strain Distribution for S7 Sample in Elastic zone at Load of 100.81 KN

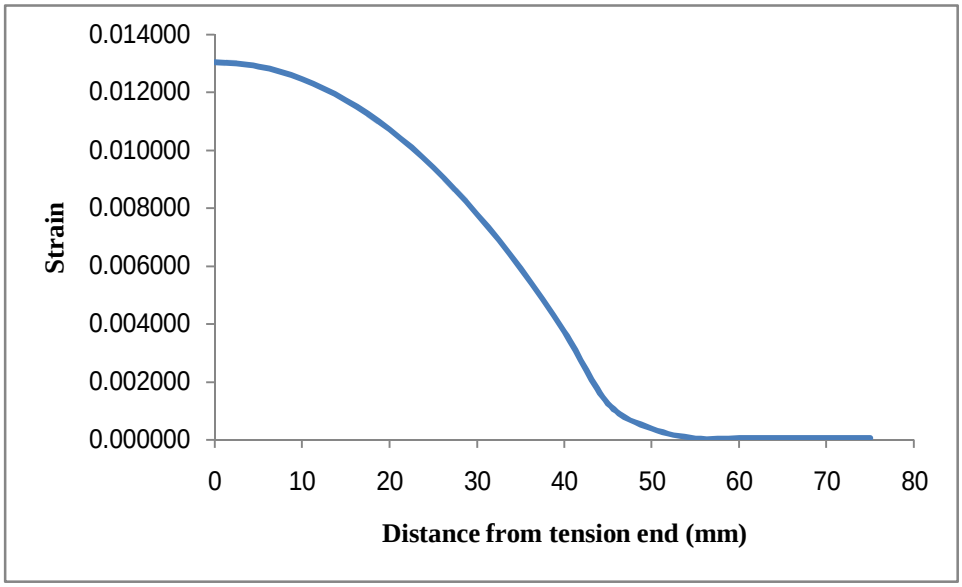

Fig. 4.23 Strain distribution for S7 Sample in Inelastic zone at Load of 124.51 KN

The strain distributions in elastic and inelastic zone are similar to those of S6 sample. In the inelastic zone curve the strain diminishes at 55 mm and hence bond length of

the specimen can be taken as 55 mm. The shear stress at failure was 6.64 N/mm^2 and greater than that of analytical value of 5.96 N/mm^2.

4.4.8 Analysis of Holed Sample S8

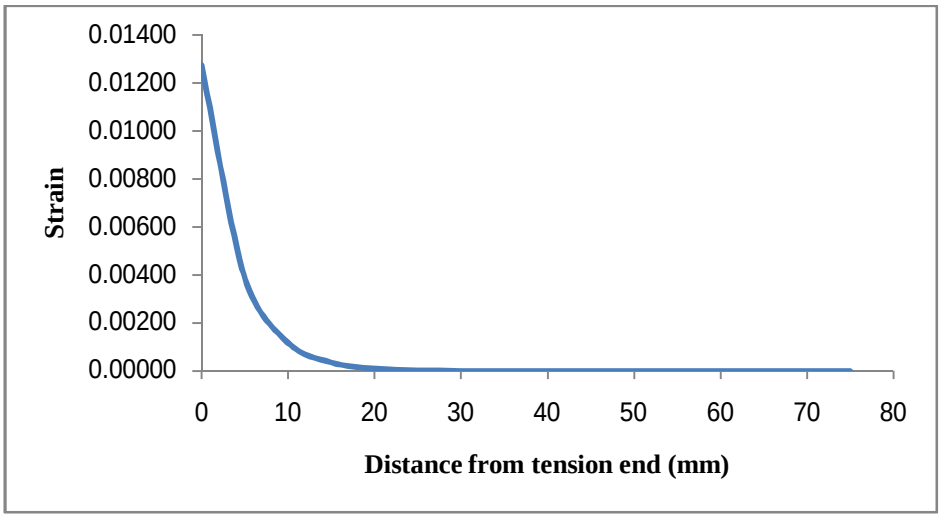

Fig. 4.24 Strain Distribution For S8 Sample In Elastic Zone at Load of 82.09 kN.

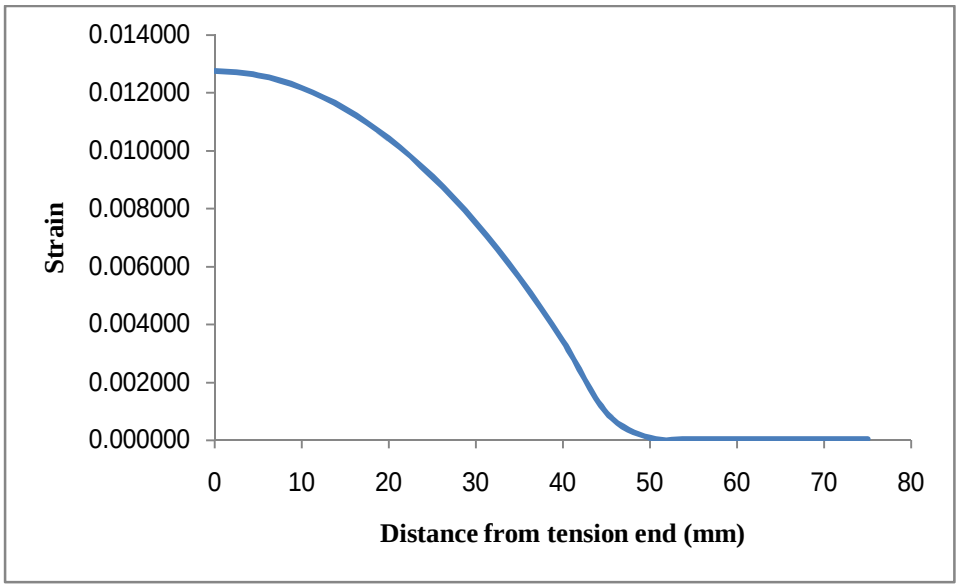

Fig 4.25 Strain Distribution for S8 sample in Inelastic Zone at Load Of 106.99 KN

Similar results were with sample S8. The strain in inelastic zone was tending zero beyond 50 mm and hence the bond length of this specimen could be taken as 50 mm The max shear stress in the experimental result was 5.706 N/mm^2 and was close to

analytical value 5.96 N/mm$^{2.}$ Therefore it can be concluded the there was no advantageous effect of providing holes in the beam. All the samples in the holed category i.e. S6,S7,S8 failed in sudden debonding at concrete epoxy interfacial zone.

4.4.9 Analysis of Sample on Damaged Beam (S9)

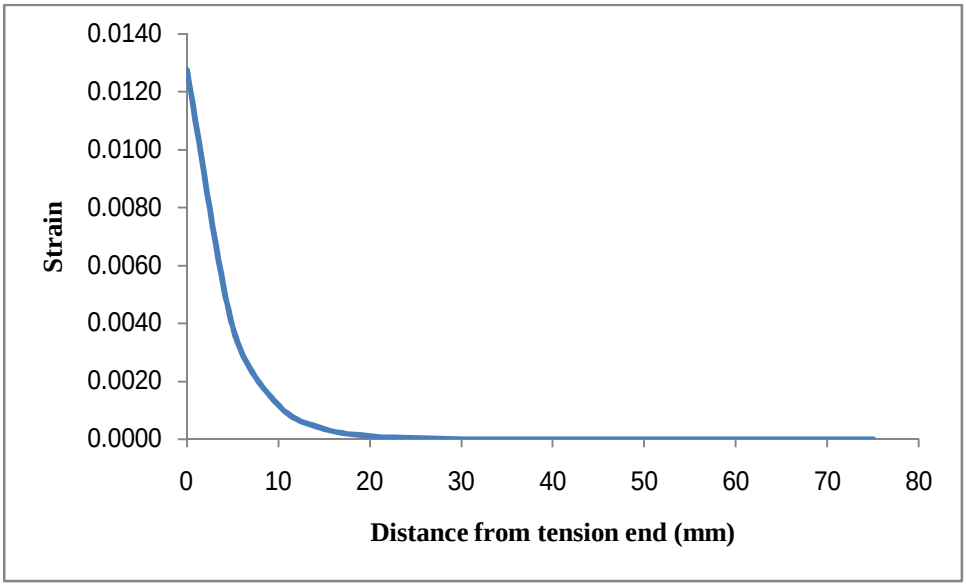

Figure4.26 Strain Distribution for S9 Sample In Elastic Zone at Load Of 45.17KN

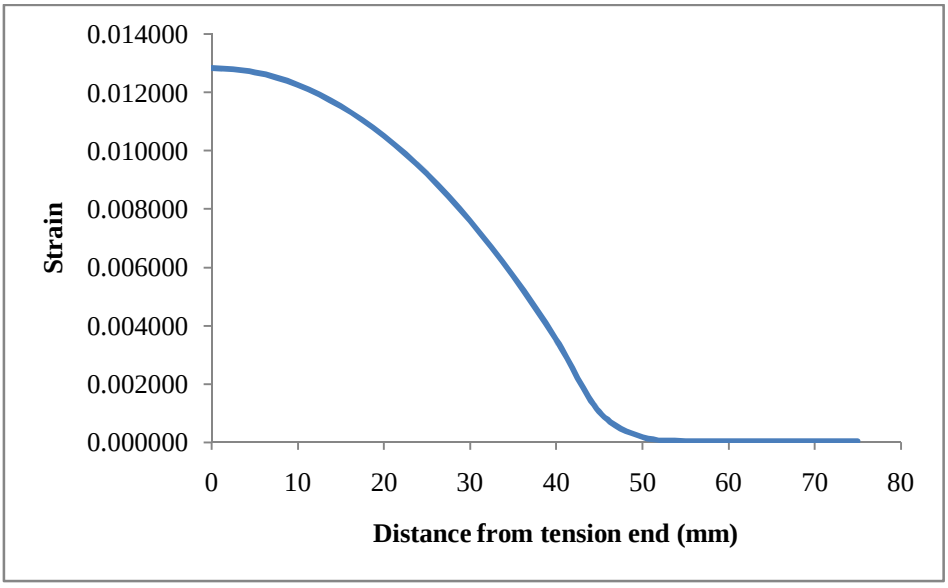

Fig 4.27 Strain Distribution for S10 Sample in Inelastic Zone at Load of 107.16 KN

Sample S9 , S10 and S11 are the samples of damaged beams. The curve in inelastic zone tends to zero beyond 52 mm and hence bond length of the specimen can be taken as 52 mm. The shear stress at failure was 5.71 N/mm^2 which is very close to the analytical model value of 5.96 N/mm^2. The failure mode was concrete shear failure.

4.4.10 Analysis of Sample on Damaged Beam (S10)

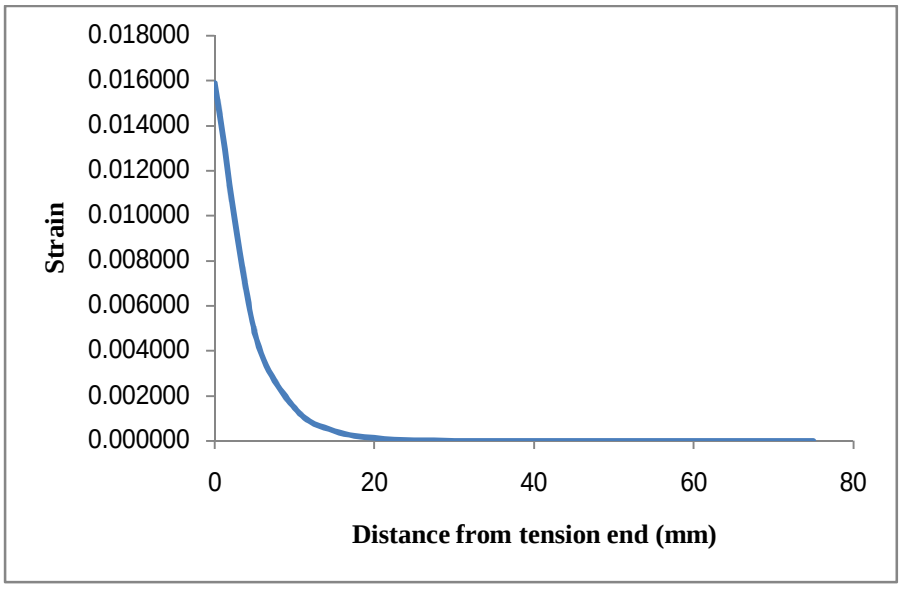

Fig4.28 Strain Distribution For S10 Sample in Elastic Zone at Load Of 99.61 KN

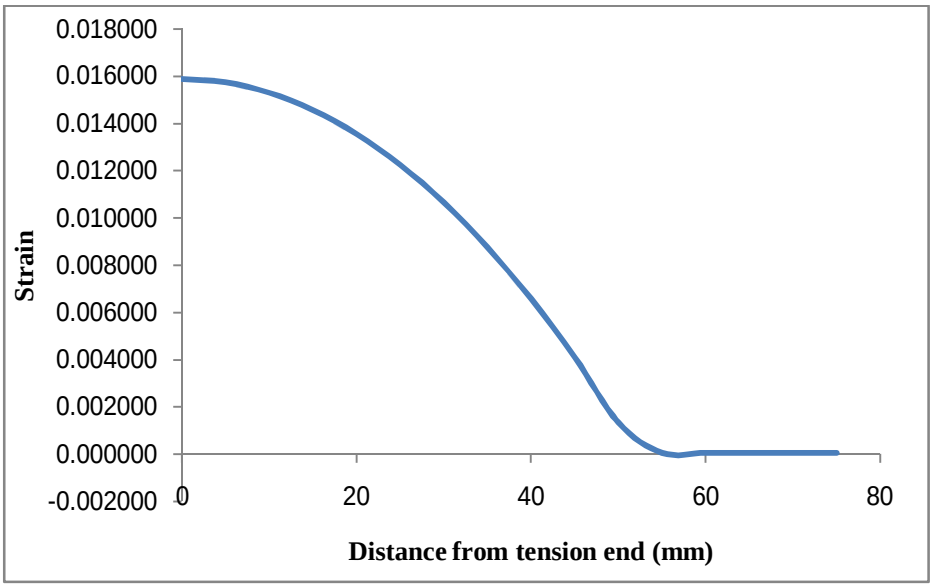

Fig 4.29 Strain Distribution for S10 sample in Inelastic zone at Load of 115.58 KN

The curve in inelastic zone diminish at 55 mm and hence the bond length of this specimen can be taken as 55m. The shear stress at which the sample failed was 6.3 N/mm^2 and is near to value of 5.96 N/mm^2 attained from analytical model. The mode of failure was shear failure in concrete.

4.4.11 Analysis of Sample on Damaged beam (S11)

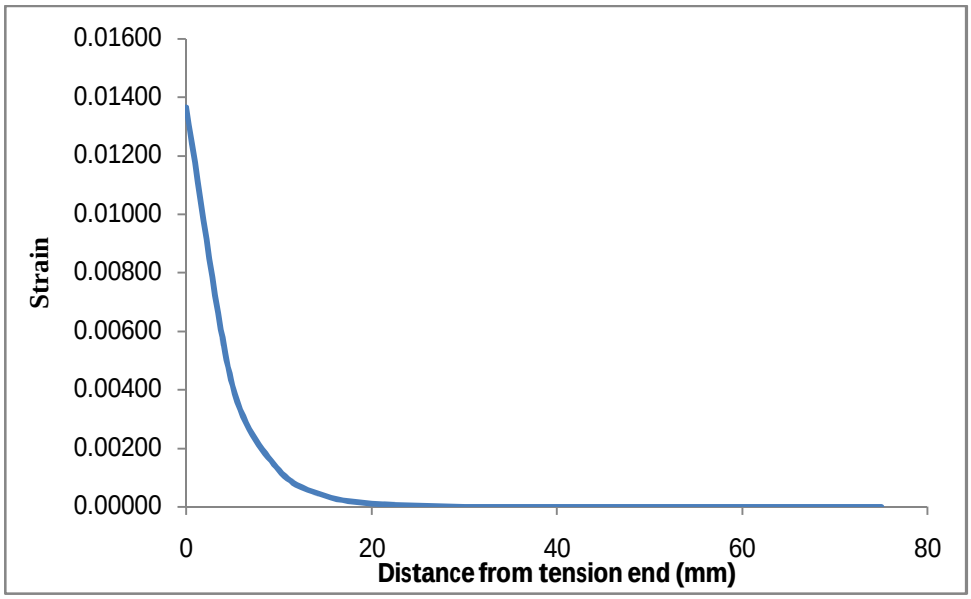

Fig 4.30 Strain Distribution for S11 Sample in Elastic zone at Load of 87.93KN

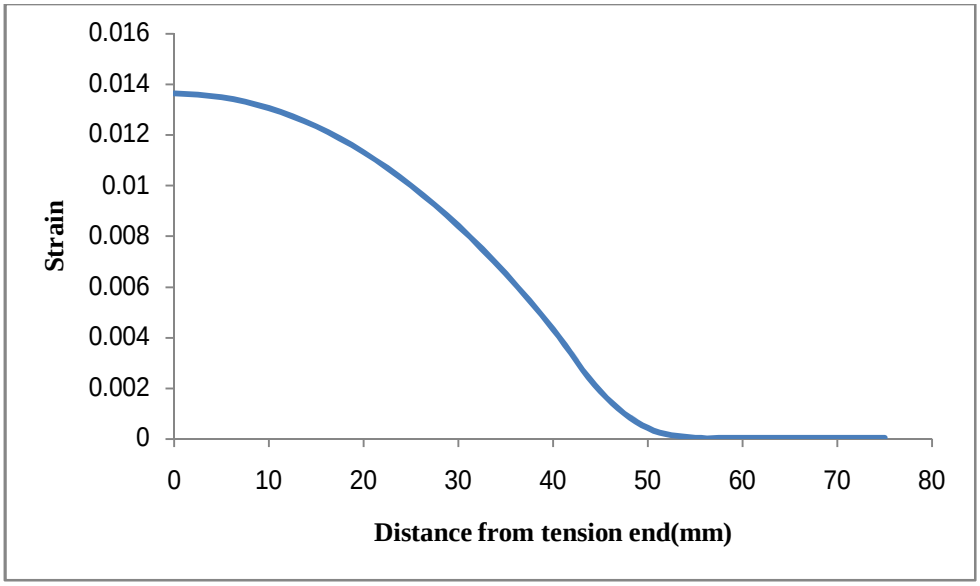

Fig 4.31Strain distribution for S11 Sample in Inelastic zone at Load of 124.33 kN

The inelastic curve tends to zero at 52 mm and thus can be taken as bond length of sample. The shear stress at failure was 6.63 N/mm^2. Which was little higher than the

analytical values. The ultimate load of failure may be in same range as that of controlled samples but the mode of failure was totally different. The controlled samples or undamaged beam failure showed only tensile cracks and eventually the ultimate strength was reached and bond failed. Moreover the damaged beam failed in shear failure of concrete. From this we can draw a conclusion that the bond strength decreases with the increase in cracks in concrete. Or bond strength is directly proportional to the tensile strength of concrete

4.5 Comparison of results with previous thesis work by Sharma. R (2013)

The thesis objective was to carry out and understand the effect of various prestressed level of CFRP on retrofitted beams. In his experiment 6 beams of size 4.1*0.6*0.3 were tested under two point loading setup. He damaged the two control beam and obtained the load vs deflection graph.

Table 4.12 Results of Test Conducted by Sharma R., (2013)

Beam state	Prestressing force % based on ultimate tensile strength of CFRP	No of CFRP	P_{UL}(KN)
Cbeam	-	1	94.35
single non prestressed	-	1	102.3
01 RDB60	60	1	126.72
02 RDB60	60	1	126
01 RDB80	80	1	146.61
02 RDB80	80	1	150

These samples were tested and failed on the loads as mentioned in the table. In our research the samples on control/undamaged beam ie sample S1, S2 and S3 were tested and the values of shear obtained must satisfy with the shear stresses generated in two point loading.

We know

$$\tau = \frac{SAy}{Ib}$$

Where τ is shear stress in the longitudinal direction

S is the ultimate load

Ay is the second moment of area

b is the width of beam in our case 600mm

I is moment of inertia

The above equation can be re written as

$$s = \frac{\tau I b}{A y}$$

From the experimental results of S1 and S2 the average shear stress

$$\tau_{avg} = \frac{\tau(S1)+\tau(S2)}{3}$$

$$\tau_{avg} = 3.53 \text{ N/mm}^2$$

$$I = b\,d^3/12 = 600*300^3/12 = 1350*10^6 \quad \text{mm}^4$$

$$y = 150 \text{ mm}$$

$$A = 600*300 = 180000 \text{ mm}^4$$

Corresponding load required to fail the sample at this shear in two point loading test will be.

$$S = 3.53*1350*10^6*600/(600*300*150)$$

S = 105.9 KN

From this result we can see the ultimate load required to produce shear stresses at failure are in accordance with the controlled beam of Sharma. R result. Hence it can be concluded that the results from the experimental studies can be used to understand the ultimate loads in flexural testing.

CHAPTER 5 CONCLUSIONS

The aim of the experiments for the present study was to compare the effect of different parameter of surface preparation and compare the results with the existing models. The shear stresses at failure in direct pull test were also compared with the shear stresses that were generated by flexural loadings. Based on the experimental results of the current study, the following conclusions may be drawn.

1. The sample in their respective group shown similar strain distribution. In inelastic zone the strain distribution beyond 50-60 mm range in all groups tends to zero. This gives the idea of bond length i.e. the length beyond which there is no effect on the value of ultimate load, hence bond length is the most effective length of the sample. Furthermore the results for each specimen were justified with the model proposed by Ming and Ansari (2004)
2. Cutting longitudinal grooves and filling them with an appropriate epoxy is an effective substitute for surface preparation, and can cause a great increase in ultimate load of beams compared to those without any surface preparation.
3. Though the ultimate loads for damaged and undamaged sample are in same range but the mode of failure is very different. The shear failure of concrete was noticed in case of damaged beams. The controlled samples on undamaged beam failure showed only tensile cracks.
4. The samples with a hole in concrete did not show appreciable results as compare to the controlled sample.
5. The experimental results of max shear stress were satisfied with Lu X J et al., (2005) model only for controlled sample. For grooved sample the experimental shear stresses were higher than that of analytical values. Hence it can be concluded the model proposed by Lu X J showed good results on fresh concrete but needs modification when used on concrete with any surface preparation.
6. The shear stress for controlled sample was compared with those of previous Thesis work by Sharma R. From the experimental values of ultimate shear stress the load was evaluated which fall the range of ultimate load of beams in the previous research.

3. ACI Committee 440, 2000, “Guide for the Design and Construction of Externally Bonded FRP Systems for Strengthening Concrete Structures,” American Concrete Institute, Farmington Hills, Mich
4. Brosens, K., & Van Gemert, D. (1999). Anchorage design for externally bonded carbon fiber reinforced polymer laminates. *ACI Special Publication*, *188*.
5. Diab, H. M., & Farghal, O. A. (2014). Bond strength and effective bond length of FRP sheets/plates bonded to concrete considering the type of adhesive layer.*Composites Part B: Engineering*, *58*, 618-624.
6. De Lorenzis, Laura, Brian Miller, and Antonio Nanni. "Bond of fiber-reinforced polymer laminates to concrete." *ACI Materials Journal* 98.3 (2001).
7. Gravina, R., S. Ali Hadigheh, and Sujeeva Setunge. "Bond and Force Transfer of FRP Materials Bonded to Concrete Using Sitecure System." *The Third Asia Pacific Conference on FRP in Structures (APFIS 2012)*. 2012
8. Kang, T. H. K., Howell, J., Kim, S., & Lee, D. J. (2012). A state-of-the-art review on debonding failures of FRP laminates externally adhered to concrete.*International Journal of Concrete Structures and Materials*, *6*(2), 123-134.
9. Lu, X. Z., Teng, J. G., Ye, L. P., & Jiang, J. J. (2005). Bond–slip models for FRP sheets/plates bonded to concrete. *Engineering structures*, *27*(6), 920-937.
10. Martin Alberto Masuelli (2013). Introduction of Fibre-Reinforced Polymers − Polymers and Composites: Concepts, Properties and Processes, Fiber Reinforced Polymers - The Technology Applied for Concrete Repair.
11. Mazzotti, C., B. Ferracuti, and M. Savoia. "An experimental study on FRP–concrete delamination." *Proc. FraMCoS, Vail USA* 2 (2004): 795-802.
12. Mazzotti, C., M. Savoia, and B. Ferracuti. "A new single-shear set-up for stable debonding of FRP–concrete joints." *Construction and Building Materials* 23.4 (2009): 1529-1537.
13. Mostofinejad, Davood, and Seyed Masoud Shameli. "Externally bonded reinforcement in grooves (EBRIG) technique to postpone debonding of FRP

sheets in strengthened concrete beams." *Construction and Building Materials*38.Complete (2013): 751-758.

14. Nakaba, K., Kanakubo, T., Furuta, T., & Yoshizawa, H. (2001). Bond behavior between fiber-reinforced polymer laminates and concrete. *ACI Structural Journal*, *98*(3).
15. Sayed-Ahmed, E. Y., Bakay, R., & Shrive, N. G. (2009). Bond strength of FRP laminates to concrete: state-of-the-art review. *Electron J Struct Eng*, *9*, 45-61.
16. Sharma, R., (2013) "Effect of prestress level on beams retrofitted with prestressed FRP sheet" M.E Thesis Thapar University Patiala.
17. Ţăranu, Nicolae, Ruxandra Oltean, and Ciprian-Ilie Cozmanciuc. "Experimental Investigation on Bonding Carbon Fiber Reinforced Polymeric Plates to Concrete Substrate."
18. Ueda, T., Sato, Y., & Asano, Y. (1999). Experimental study on bond strength of continuous carbon fiber sheet. *ACI Special Publication*, *188*.
19. Wan, B., Petrou, M. F., Harries, K. A., Sutton, M. A., & Yang, B. (2002). Experimental investigation of bond between FRP and concrete. In *3rd Int. Conf. on Composites in Infrastructures ICCI'02*.
20. Zhao, Ming, and Farhad Ansari. "Bond properties of FRP fabrics and concrete joints." *Proc., 13th World Conf. on Earthquake Engineering*. 2004.